Master of Science Thesis in Electrical Engineering
Department of Electrical Engineering, Linköping University, 2020

Steering Control During μ-split Braking for an Autonomous Heavy Road Vehicle

Sebastian Haglund and Henrik Johansson

LINKÖPING UNIVERSITY

Master of Science Thesis in Electrical Engineering

Steering Control During μ-split Braking for an Autonomous Heavy Road Vehicle:

Sebastian Haglund and Henrik Johansson

LiTH-ISY-EX--20/5304--SE

Supervisors: **Victor Fors**
ISY, Linköping university
Linus Flodin
Scania CV AB
Ahmet Arikan
Scania CV AB

Examiner: **Jan Åslund**
ISY, Linköping university

Division of Vehicular Systems
Department of Electrical Engineering
Linköping University
SE-581 83 Linköping, Sweden

Abstract

A critical maneuver for a heavy vehicle is braking with different friction on the left and right hand side of the vehicle, called μ-split. This results in an unwanted yaw torque acting on the vehicle. During this situation, the driver maintains the lateral stability and follows the desired path by corrective steering. In an autonomous heavy vehicle the system must handle this situation by itself. The purpose of this thesis is to analyze how an autonomous vehicle can detect a μ-split situation and then use steering control to maintain its path and stability.

Two methods for detecting a μ-split situation are presented where one is based on vehicle kinematics, this detector utilizes the difference in wheel speed between the left and right hand side of the vehicle. The other detector is based on lateral vehicle dynamics, this method uses a sliding mode observer to detect unexpected changes in the yaw rate signal. The detectors were tested in a real vehicle and the results showed that the kinematic detector was fast but had a small risk of false detection, while the dynamic detector was slower but more robust.

An analysis of the desired steering behavior showed that the steady state during μ-split braking is to drive with a non zero body slip. If a kinematic path follower is used with kinematic error dynamics this will lead to a contradicting behavior since the body slip is equal to the heading error during straight line braking, assuming that the velocity vector of the vehicle is parallel to the path.

Simulations showed that during a μ-split situation the Linear Quadratic path follower based on kinematic error dynamics manages to follow the path with a non zero body slip while keeping the path errors small. It has also been shown how the detection of a μ-split situation can be used to change control strategy. By introducing active yaw control or change the tuning on the controller after a detection a better result could be achieved.

Acknowledgments

First of all we would like to thank our supervisors at Scania CV AB Linus Flodin and Ahmet Arikan. Thank you for your support and guidance throughout this period and for taking us out on the test track. We would also like to thank our supervisor at Linköping university Victor Fors for all the great feedback on the report and your valuable inputs. We would like to thank our examiner Jan Åslund. Lastly we would like to thank Scania CV AB and all great people working there.

Linköping, May 2020
Sebastian Haglund and Henrik Johansson

Contents

Notation

Notation	Description
μ	Friction coefficient
ω	Wheel angular velocity
a	Acceleration
v	Velocity
F	Force
Ω	Yaw rate
δ	Steering angle
s	Longitudinal slip
R	Radius
α	Slip angle
β	Body slip angle
m	Mass
l	Length
h	Height
g	Gravitational constant
A	Cross sectional area
ρ	Density
C_d	Drag coefficient
C_α	Cornering stiffness
d	Lateral deviation
θ	Angle
I	Moment of inertia
M	Torque
K_b	Brake force distribution

Abbreviations

Abbreviation	Description
ABS	Anti-lock braking system
AFS	Active front steering
AYC	Active Yaw Control
CUSUM	Cumulative sum
ESP	Electronic Stability Program
GNSS	Global Navigation Satellite System
GPS	Global Positioning System
LQR	Linear-Quadratic Regulator
MPC	Model Predictive Control
PF	Path Follower
PPC	Pure-Pursuit Controller
SMO	Sliding Mode Observer

1 Introduction

When performing aggressive dynamical maneuvers with a heavy road vehicle, one of the most important things to consider is the vehicle stability. These maneuvers can cause dangerous situations such as roll-over, trailer-swing and jack-knifing, which can lead to serious accidents. One critical situation for heavy road vehicles is braking with different friction on the left- and right-hand side, called μ-split. There are systems designed to help the driver stabilize the vehicle during critical situations and ensure a short stopping distance. In the case of μ-split braking, the brake system will try to maximize the brake force at each wheel. This will lead to an uneven force distribution between the left- and the right-hand side of the vehicle, generating a yaw torque which jeopardizes the vehicle stability. To avoid this, the brake system only allows a certain amount of yaw torque. To make sure the vehicle keeps its heading and does not becomes unstable, the driver has to compensate for the yaw torque. The driver will detect the μ-split situation and then counter steer to maintain stability. An autonomous system has to handle this without the help of a driver. The system must be able to detect a μ-split situation by itself, compute a proper amount of counter steering and send it to the actuators to ensure vehicle stability.

1.1 Purpose and Problem Formulation

The purpose of this thesis is to investigate a μ-split braking situation. A system that can handle μ-split braking for autonomous heavy road vehicles should be developed and evaluated. The system should include a controller that uses the steering actuator to maintain vehicle lateral stability during braking. The system should also be able to detect a μ-split braking situation using the sensors on the tractor.

- How can a robust detector be designed to detect a µ-split situation sufficiently fast for the controller to stabilize the vehicle?
- How can a steering controller be designed for an autonomous heavy road vehicle to maintain stability and heading during μ-split braking?

1.2 Related Work

This section gives a short summary of relevant and related research to this thesis.

1.2.1 Control of Autonomous Vehicles

The high level control of autonomous vehicles is often based on following a given path. There are several different methods and approaches for solving the path following problem. Some control strategies for path following are: Pure-pursuit controller (PPC), Model predictive controller (MPC), and Linear-quadratic regulator (LQR) [16].

The research about autonomous vehicles during critical maneuvers often incorporates the lateral stability in the path following problem. In [8], a yaw controller is developed with the purpose of being used in autonomous vehicles. This controller both stabilises the vehicle and minimizes the path deviation. The path following problem can be transformed into a yaw- and lateral velocity control problem. The problem is solved by calculating the desired yaw rate from the lateral offset and the heading error as done in [10].

1.2.2 Stability Control During µ-split Braking

Stability of heavy road vehicles is a widely studied topic. During μ-split braking the balance between stopping distance and lateral stability must be considered. There are several methods to ensure the stability of a heavy road vehicle. In [20], a LQR is used for differential braking to prevent jackknifing and rollover. Another approach to maintain stability is to use Active Front Steering (AFS) as done in [22]. This method uses the wheel velocities to compute the unwanted yaw torque from the Anti Lock braking System (ABS) when braking under μ-split conditions. To compensate for the unwanted yaw torque, the controller uses counter steering of the front axle. More advanced controllers such as MPC has also been used for truck stability. In [11], a MPC was able to reduce the yaw amplification from truck to the semitrailer in a truck-dolly-semitrailer combination.

In [18], a sliding mode controller was developed to maintain stability during μ-split braking. The lateral offset from the desired trajectory is included as a state in the model. The lateral deviation is computed by the relative position to the road markings with a vision system. The proposed controller shows good results in terms of reducing yaw rate and lateral offset. It also shows good robustness to parameter uncertainties. In [2], the authors combine the ABS system with a steering controller to minimize the stopping distance while maintaining vehicle

stability during μ-split braking. When a μ-split situation is detected, the detector sends a command to the brake system to disable the pressure attenuation, the same signal initializes the steering controller. The steering controller then use information from the measured yaw rate and brake pressures to take the necessary actions to maintain stability. In [1], the authors design a steering controller that uses feedback from the disturbance yaw rate to adjust the steering angle. This is done to compensate for the unexpected yaw rate generated by μ-split braking.

1.2.3 Detection of µ-split Situation

There are several approaches to detect a μ-split situation. One approach is to estimate the friction coefficient and then compare the left-hand side to the right-hand side. To estimate the friction a slip based approach can be used as done in [7]. The method is based on a Kalman filter where the relative slip slope is estimated. Another approach to estimate the friction is to use neural networks. The authors in [13] proposes a radial basis neural network in the estimation of road friction, to get a more robust estimation less sensitive to model errors.

Another way of detecting a μ-split situation is described in [5], where the authors don't explicit try to estimate the vehicles states, yaw rate and lateral acceleration. Instead the measured behavior of the vehicle is compared to the expected behavior from a linear model. The method is based on the idea that unexpected yaw torque and lateral acceleration will appear during oversteering, understeering and μ-split braking. In the case of a μ-split braking one could expect an initial peak in the unexpected yaw torque.

In [2], the μ-split detection is done using a detector that monitors the brake pedal signal and brake pressure. When the brake pedal is active and the difference in brake pressure between the left and right wheels exceeds a certain value the detector identifies a μ-split situation.

There are methods that uses neural networks. In [12] the authors uses a extended state observer to estimate the vehicle states and the unknown dynamics. The unknown dynamics are then used to estimate and classify the road surface conditions which is done by using fuzzy logic and a neural network.

1.3 Limitations

There are many different heavy road vehicles and in this thesis only a tractor will be considered. The tractor to be investigated is a 4x2 tractor. This tractor has two axles where the front axle is the steering axle and the rear axle is the driven axle. Only braking on straight roads are considered with constant μ-split. This means that one side has constant low friction while the other has constant high friction. Since the test vehicle does not have all sensors one could expect from an autonomous vehicle this limits the possible methods of detecting a μ-split situation to only use available sensor data.

1.4 Thesis Outline

- **Chapter 1 - Introduction** presents the problem and background to this thesis. The purpose of the thesis is stated with relevant research connected to the subject.
- **Chapter 2 - Theory** presents relevant theoretical areas used in this thesis, this includes vehicle dynamics, signal processing and control theory.
- **Chapter 3 - Detection of µ-Split Situation** describes the braking behavior during a μ-split braking and two proposed detectors are presented, one based on vehicle kinematics and one on vehicle dynamics.
- **Chapter 4 - Simulation Environment for Controller Development** presents how the simulation environment is constructed and how it is used. The main purpose of the simulation environment is to evaluate different control algorithms. The simulation environment is validated by comparing simulation results to real world test data.
- **Chapter 5 - Steering Control** presents an analysis of the desired steering behavior during μ-split braking. Control strategies that could be used to handle the steering and stability are also presented.
- **Chapter 6 - Results** presents the results from real world test of the μ-split detectors. The results from test of the controllers in the simulation environment are also presented.
- **Chapter 7 - Discussion and Conclusions** contains a discussion of the results. Conclusions based on the results for both the detectors and the control strategies are presented. Suggestions for future work based on this thesis are also presented.

2
Theory

The theoretical presumptions that this theses is based on are presented in this chapter. The main theoretical areas are: vehicle kinematics and dynamics, control theory and signal processing.

2.1 Vehicle Kinematics and Dynamics

To analyze and design systems for vehicles there is a need for understanding the vehicle behavior. One way to describe the behavior is by using mathematical models. In this thesis a lot of analysis and system design concerns the vehicle behavior. In following sections the theory needed for this are presented.

2.1.1 Kinematic Error Dynamics

An autonomous vehicle will move in a global coordinate system. The high level motion control is based on following a given path. If the vehicle does not follow the path perfectly there will be path errors described by two variables, d and θ_e. Where d is the distance from the path and θ_e is the heading error, which is the difference between the vehicle heading, θ, and the path heading, θ_s. The kinematic path errors are illustrated in Fig. 2.1, where θ_s is the path heading in global coordinates. From this the non-linear error dynamics can be derived as

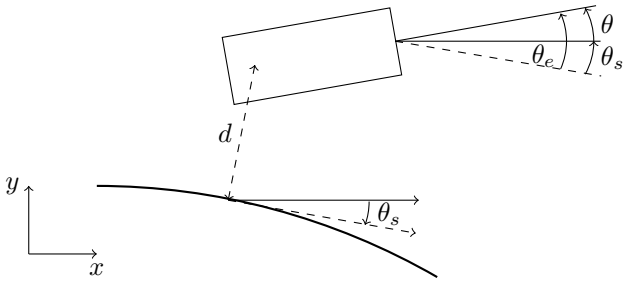

Figure 2.1: *The figure shows the errors of a vehicle during path following.*

$$\begin{aligned} \dot{s} &= \frac{v}{1 - dc(s)} \cos(\theta_e) \\ \dot{d} &= v \sin(\theta_e) \\ \dot{\theta}_e &= vu - \dot{s}c(s) \\ u &= \frac{1}{l_f + l_r} \tan \delta \end{aligned} \tag{2.1}$$

where v is the vehicle velocity, $c(s) = \frac{1}{R_p}$ is the path curvature, R_p is the curve radius, s is the curvilinear abscissa obtained by projecting the point on the vehicle orthogonal on the path, u is the chassis instantaneous rotational velocity and δ is the steering angle [19].

The definitions of the heading error and lateral error are valid when driving straight or in moderate curves. In paths with great curvature or changing curvature the heading error can not be equal to zero if the lateral offset is equal to zero and vice versa. This is due to the fact that the definition in (2.1) does not consider the vehicle body slip. This will lead to larger heading error during these kinds of situations and it will be harder to converge the lateral error to zero. This effect could be reduced by considering the body slip in the heading error. By taking this into consideration it becomes possible to converge both the lateral error and the heading error to zero at the same time, which could result in a more accurate control [9].

2.1.2 Single-Track Model

The motion of a tractor can be modeled with a single-track model also known as the bicycle model shown in Fig. 2.2. This model is often used when analyzing lateral motion of a vehicle and it is also used in simple Electronic Stability Programs (ESP). An assumption in the model is that the center of mass is located in the plane that the vehicle travels on. This results in that no load transfer will occur during driving, which is the reason that the model lumps the wheels on the same axle together [14].

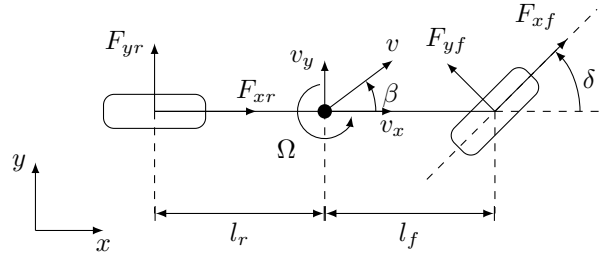

Figure 2.2: *A bicycle model of the tractor where x and y is the body coordinate system.*

The equations of motion of the model in Fig. 2.2 are derived using Newtons second law, where the linear tire model in (2.10) is used. The resulting equations are

$$\begin{aligned} m(\dot{v}_y + v_x\Omega) &= 2C_{\alpha r}\alpha_r + 2C_{\alpha f}\alpha_f \cos(\delta) + 2F_{xf}\sin(\delta) \\ I_z\dot{\Omega} &= 2l_f(C_{\alpha f}\alpha_f \cos(\delta) + F_{xf}\sin(\delta)) - 2l_r C_{\alpha r}\alpha_r \end{aligned} \tag{2.2}$$

where m is the vehicle mass, Ω is the yaw rate, δ is the steering angle, F_{xf} is the longitudinal force at the front wheel, I_z is the moment of inertia, l_f and l_r are the lengths defined in Fig. 2.2. The sub indices r stands for rear and f for front.

Single Track Model Kinematics

By using kinematic relationships the lateral and longitudinal velocities of each wheel can be obtained. These are needed for modeling the lateral force described in Sec. 2.1.5. The resulting velocities are

$$\begin{cases} v_{xf} &= v_x \\ v_{yf} &= v_y + l_f\Omega \end{cases} \qquad \begin{cases} v_{xr} &= v_x \\ v_{yr} &= v_y - l_r\Omega \end{cases} \tag{2.3}$$

Body Slip Angle

The body slip angle is the angle between the heading of the vehicle and the direction of the vehicle velocity [14]. This can be described as the angle between the lateral and longitudinal velocity components of the vehicle velocity v. The body slip angle, β, can be seen in Fig. 2.2 and it can be calculated using

$$\beta = \arctan\left(\frac{v_y}{v_x}\right) \tag{2.4}$$

where v_y is the lateral velocity of the vehicle and v_x is the longitudinal velocity [17].

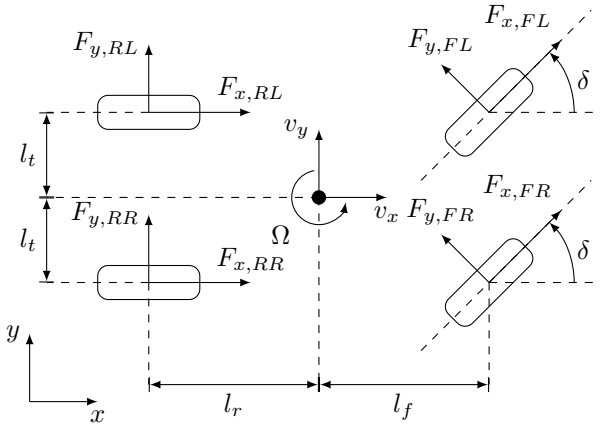

Figure 2.3: *A four wheel model of the tractor where x and y is the body coordinate system.*

2.1.3 Four-Wheel Model

A more complex model than the single track model is a four-wheel model. This model can be seen in Fig. 2.3. This model introduces the possibility to model uneven behavior between the left and right side of the vehicle, this is useful when describing a μ-split behavior. The equations of motion are

$$\begin{aligned}
m(\dot{v}_x - v_y\Omega) =& F_{xFL}\cos(\delta) + F_{xFR}\cos(\delta) - F_{yFL}\sin(\delta) \\
&- F_{yFR}\sin(\delta) + F_{xFL} + F_{xFR} \\
m(\dot{v}_y + v_x\Omega) =& F_{xFL}\sin(\delta) + F_{xFR}\sin(\delta) + F_{yFL}\cos(\delta) \\
&+ F_{yFR}\cos(\delta) + F_{yRL} + F_{y,RR} \\
I_z\Omega =& (F_{x,FR}\cos(\delta) - F_{xFL}\cos(\delta) + F_{xRR} \\
&- F_{xRL} + F_{yFL}\sin(\delta) - F_{yFR}\sin(\delta))l_t \\
&+ (F_{xFL}\sin(\delta) + F_{xFR}\sin(\delta) + F_{yFL}\cos(\delta) + F_{yFR}\cos(\delta))l_f \\
&- (F_{yRL} + F_{yRR})l_r
\end{aligned} \tag{2.5}$$

where l_t is half the track width and F are the forces acting on the tires, defined in Fig. 2.3.

Air Resistance

In the equation for longitudinal dynamics in (2.5) the air resistance is not modeled. During driving the air resistance will cause a drag force acting in the opposite direction of the vehicle velocity. The drag force is calculated using

$$F_D = \frac{1}{2}C_D\rho A v^2 \tag{2.6}$$

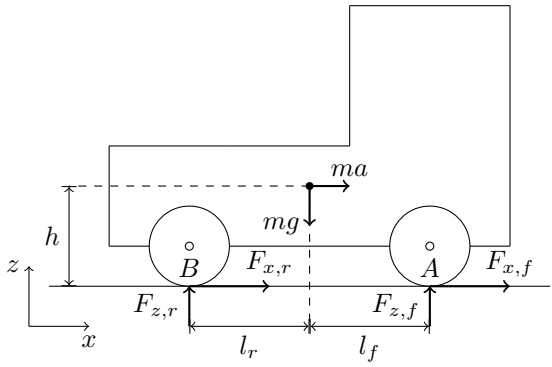

Figure 2.4: *A free body diagram of the tractor.*

where the force depends on the drag coefficient, C_D, the density of the surrounding fluid, ρ, the cross sectional area, A, and the velocity, v [21].

2.1.4 Load Transfer

The single-track model and the four-wheel model does not consider the load transfer that occurs when a vehicle is subjected to acceleration or deceleration. The normal force distribution will change during these events. The sum of the torque acting around point A and B in Fig. 2.4 is used to derive the expression

$$\begin{aligned} F_{z,f} &= mg\left(\frac{l_r}{l_r + l_f} - \frac{ah}{g(l_f + l_r)}\right) \\ F_{z,r} &= mg\left(\frac{l_f}{l_r + l_f} + \frac{ah}{g(l_f + l_r)}\right) \end{aligned} \tag{2.7}$$

where $F_{z,f}$ is the normal load at the front axle, $F_{z,r}$ is the normal load at the rear axle and h is the height to the center of gravity. The first part of the expression is the influence of static load and the second part of the expression is the influence of load transfer during acceleration or deceleration [21].

Contact Force

The maximum contact force a tire can deliver to the road surface can be determined by the normal force, F_z, and the friction coefficient, μ and can be calculated using

$$F_{max} = \mu F_z \tag{2.8}$$

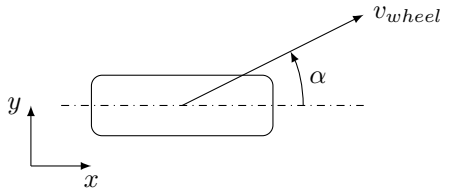

Figure 2.5: *The figure shows the slip angle and its connection to the wheel plane and velocity vector.*

2.1.5 Wheel Model

In the single-track model and the four-wheel model there are forces acting on the wheels. The longitudinal force will be used as an input in the simulation environment later in the thesis and does therefor not need to be modeled. The lateral forces can be modeled as described in this section.

Side Slip Angle

When a tire is exposed to lateral forces it will not move in the direction of the wheel plane. Instead it will move in an angle, α, called side slip angle. The slip angle is defined as the angle between the velocity vector of the wheel and the wheel plane, as can be seen in Fig. 2.5 [21]. The angle can be calculated using

$$\alpha = -\arctan\left(\frac{v_{y,wheel}}{v_{x,wheel}}\right) \tag{2.9}$$

where $v_{x,wheel}$ and $v_{y,wheel}$ are the components of the velocity vector v_{wheel}.

Cornering Stiffness

The magnitude of lateral force a tire can deliver depends on the cornering stiffness, C_α, and the slip angle, α. The lateral force is calculated with

$$F_y = C_\alpha \alpha \tag{2.10}$$

The cornering stiffness is defined as the derivative of the cornering force, F_y, with respect to the slip angle as seen below

$$C_\alpha = \frac{\partial F_y}{\partial \alpha}\bigg|_{\alpha=0} \tag{2.11}$$

For small slip angles the cornering force is approximately proportional to the slip angle, as the side slip angle increase the cornering force becomes saturated [21].

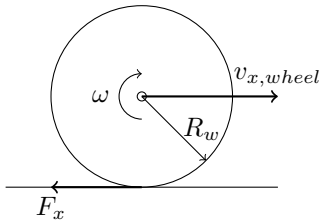

Figure 2.6: *Forces and kinematics on a rolling wheel with applied braking torque.*

Friction ellipse

When a tire is exposed to lateral and longitudinal forces the friction ellipse is used to determine the available force in the different directions. This can be used as saturation to the lateral tire forces since the model in (2.10) does not model this saturation. The equation for the ellipse is

$$\left(\frac{F_y}{F_{ymax}}\right)^2 + \left(\frac{F_x}{F_{xmax}}\right)^2 \leq 1 \tag{2.12}$$

where F_{xmax} and F_{ymax} is the maximum available force in the longitudinal and lateral direction and F_x and F_y are the forces the tire is exposed to. During steady state cornering the maximum force the tire can deliver in the lateral direction is F_{ymax}. If a braking torque is applied during cornering the amount of lateral force the tire can produce will decrease [21].

Longitudinal Slip

When a braking torque is applied to a wheel, a tractive force is generated at the contact patch between tire and ground as illustrated in Fig. 2.6 [21]. This results in a difference in velocity between the vehicle and the wheel, because the tire is sliding on the ground. This sliding between the wheel and the ground is called slip. The slip is calculated with

$$s = \frac{v_{x,wheel} - R_w\omega}{v_{x,wheel}} \tag{2.13}$$

where $v_{x,wheel}$ is the wheel velocity, ω is the wheel angular velocity and R_w is the wheel radius. During braking the slip varies between zero and one, were zero slip is a free rolling tire and one is a locked wheel.

2.2 Signal Processing

In a vehicle there are several signals used to track the vehicle behavior. By using signal processing useful information about the vehicle could be found in these signals.

2.2.1 Sliding Mode Observer

A sliding mode observer (SMO) is a discontinuous observer and has the form

$$\dot{\hat{x}} = A\hat{x} + B\bar{u} + L\text{sign}(\bar{y} - C\hat{x}) \tag{2.14}$$

where A, B and C are matrices describing the dynamic system, $\hat{x}$ is the estimated state variables, $\bar{y}$ is the measured signals, $\bar{u}$ is the input signals and L is the gain matrix. The matrix L should be chosen such that sliding occurs on the manifold $\bar{y} - C\hat{x} = 0$. Once sliding is obtained the state observer in (2.14) will track the measured signals $\bar{y}$ perfect [4].

2.2.2 CUSUM

A cumulative sum (CUSUM) algorithm is an algorithm used to detect changes in data. It is based on the log-likelihood ratio

$$\lambda = \ln \frac{p_{\theta_1}}{p_{\theta_0}} \tag{2.15}$$

where p_{θ_0} and p_{θ_1} are normal distributions with different mean values. Given a positive change in θ the log-likelihood ratio will have the properties that the expected value is less than zero if there is no change in the mean value and greater than zero if there is a positive change. This can be formulated as

$$\begin{aligned} E\{\lambda\} < 0, \quad \theta = \theta_0 \\ E\{\lambda\} > 0, \quad \theta = \theta_1 \end{aligned} \tag{2.16}$$

The properties in (2.16) result in that λ will have a negative drift before a change in the mean value and a positive drift after a change. This result is used in the algorithm below

$$\begin{aligned} T_k &= \max\{0, S_k - m_k\} > limit \\ S_k &= \sum_{i=1}^{k} \lambda_i \\ m_k &= \min_{1 \le j \le k} S_j \end{aligned} \tag{2.17}$$

where S_k is the cumulative sum, m_k is an adaptive threshold, $limit$ is a constant threshold and T_k is the test quantity [3].

In [15] a CUSUM algorithm that works together with residuals is presented. The value of the residual should be zero during a fault free case and non zero if there is a fault. If a residual is used the properties in (2.16) are no longer valid. By introducing a drift factor ϕ, the test becomes

$$T_k = \max\{0, T_{k-1} + |r_k| - \phi\} \tag{2.18}$$

where T is the test quantity and r is the residual. If there is large model uncertainties in some regions ϕ could be used as an adaptive parameter. The parameter ϕ should be in the same order of magnitude as the residual during a fault free case.

2.3 Linear-Quadratic Regulator

In order to control the motion of a vehicle a controller is needed. A LQR is a controller that is based on optimal control theory. LQR is a widely studied topic within control theory and one description can be found in [6]. The goal is to control a dynamic system by minimizing a quadratic cost function. The dynamic system can be described as

$$\begin{aligned} \dot{\bar{x}} &= A\bar{x} + B\bar{u} + N\bar{v}_1 \\ \bar{z} &= M\bar{x} \\ \bar{y} &= C\bar{x} + \bar{v}_2 \end{aligned} \tag{2.19}$$

where A, B and C are matrices describing the dynamic system, $\bar{x}$ is the state variable vector, $\bar{y}$ is the measured signals, M is a matrix describing which states that are supposed to be controlled where $\bar{z}$ is the controlled states and $\bar{v}_1$ and $\bar{v}_2$ are white noise. The quadratic cost function depends on both the control signals, $\bar{u}$, and the error signals, $\bar{e}$, where $\bar{e} = \bar{z} - \bar{r}$. By assuming $M = I$ and $r = 0$ then $\bar{e} = \bar{x}$. The objective function then becomes

$$\min(\|\bar{x}\|^2_{Q_1} + \|\bar{u}\|^2_{Q_2}) = \min \int \bar{e}^\intercal(t) Q_1 \bar{e}(t) + \bar{u}^\intercal(t) Q_2 \bar{u}(t)\, \mathrm{d}t \tag{2.20}$$

where Q_1 is a positive semidefinite matrix and Q_2 is a positive definite matrix. These matrices are weight matrices and can be seen as tuning parameters for the controller. The optimal linear feedback that minimizes (2.20) is

$$\begin{aligned} \bar{u}(t) &= -L\bar{x}(t) \\ L &= Q_1^{-1} B^\intercal S \end{aligned} \tag{2.21}$$

where S is the solution to the Riccati equation. The Riccati equation can be written as

$$A^\intercal S + SA + M^\intercal Q_1 M - SBQ_2^{-1} B^\intercal S = 0 \tag{2.22}$$

The solution S to the equation is a symmetrical, unique and positive semidefinite matrix.

3

Detection of μ-Split Situation

In this thesis, two μ-split detectors have been investigated and evaluated. The detectors are presented in this chapter. The kinematic detector is based on the fact that there is a difference in slip on the left- and right-hand side during μ-split braking, while the dynamic detector is based on the fact that there will be an unexpected yaw torque on the vehicle. The two methods uses different sensors to detect a μ-split situation.

3.1 Braking Behavior

The following section contains a description of the ABS. The section also explains the differences in braking on high friction, low friction and split friction surfaces.

3.1.1 Anti-Lock Braking System

To maximize brake performance, heavy vehicles are equipped with ABS. By preventing the wheels from locking a higher tractive force can be maintained during braking minimizing the stopping distance. The ABS works to keep the slip at a certain level where the tire can generate the maximum amount of longitudinal force to the ground and maintain lateral control of the vehicle. To maintain stability the brake system only allows a certain amount of slip difference between the left and right side of the vehicle. If this amount is exceeded the system will lower the actuated brake force on the low slip side. There is also a maximum brake force difference allowed between the two sides, if this difference exceeds a certain value the high brake force side will be lowered to minimize the generated yaw torque.

3.1.2 Braking with ABS

When braking on a μ-split surface the amount of brake force between the tire and ground reduces drastically on the low-μ side while the brake force remains large at the high-μ side. This behavior can be seen in (2.5) and Fig. 2.3. If there is a higher braking force on the left hand side, F_{xFL} and F_{xRL} will be greater than F_{xFR} and F_{xRR}. The uneven force distribution on the vehicle generates a yaw torque around the center of mass of the vehicle, making it rotate towards the high-μ side. In Fig. 3.1 the different behaviors between typical high-μ, low-μ and μ-split brakings can be seen. For the high-μ braking the velocity of both wheels closely follows the actual vehicle velocity. During low-μ-braking both wheels struggle to maintain traction leading to high slip values. The μ-split situation is a combination of these two, where the high-μ wheel has small variations in slip while the low-μ wheel has large variations.

This behavior can also be seen in Fig. 3.2. For high- and low-μ braking the mean value of the yaw rate remains around zero during braking, while during a μ-split braking the yaw rate starts to drift. This is a consequence of the uneven force distribution. The driver will however counter steer to stabilize the tractor and that is why the drift suddenly stops.

3.2 Kinematic Detector

The kinematic μ-split detector is based on the longitudinal wheel slip. The global velocity of the vehicle is measured by the Global Positioning System (GPS) receiver or Global Navigation Satellite System (GNSS) receiver. The wheel velocities are measured by the wheel speed sensors. From this data the slip for the front wheels are computed. There are several reasons that the slip of the front wheels is used, one is due to quicker ABS control for the front wheel pair and that the ABS control of the front wheels is also more consistent between different tractor configurations. The last reason is that the brake configuration in the front is the same for all models while it varies a lot in the rear between different tractor configurations. The detector receives the computed slip values and compares the difference in slip to a threshold. If the difference in slip exceeds the threshold a μ-split alarm is set. To avoid false alarm during normal driving, the brake needs to be activated for the detector to be enabled. In Fig. 3.3 a block diagram describing the process can be seen.

As seen in (2.13), when the rotational velocity of the wheels converges to zero the slip will converge to 1 leading to peaks in the slip values. These peaks are used to identify a μ-split situation. However at low velocity the slip converges to 1 as well, which will lead to false detection. Therefore a velocity limit has been set, when the velocity is below this limit the detector will disconnect to prevent false detection. Due to the fact that the lateral dynamics are more stable at lower velocities and the short stopping distance it is assumed that there is no need to detect μ-split situations at velocities below 20 km/h.

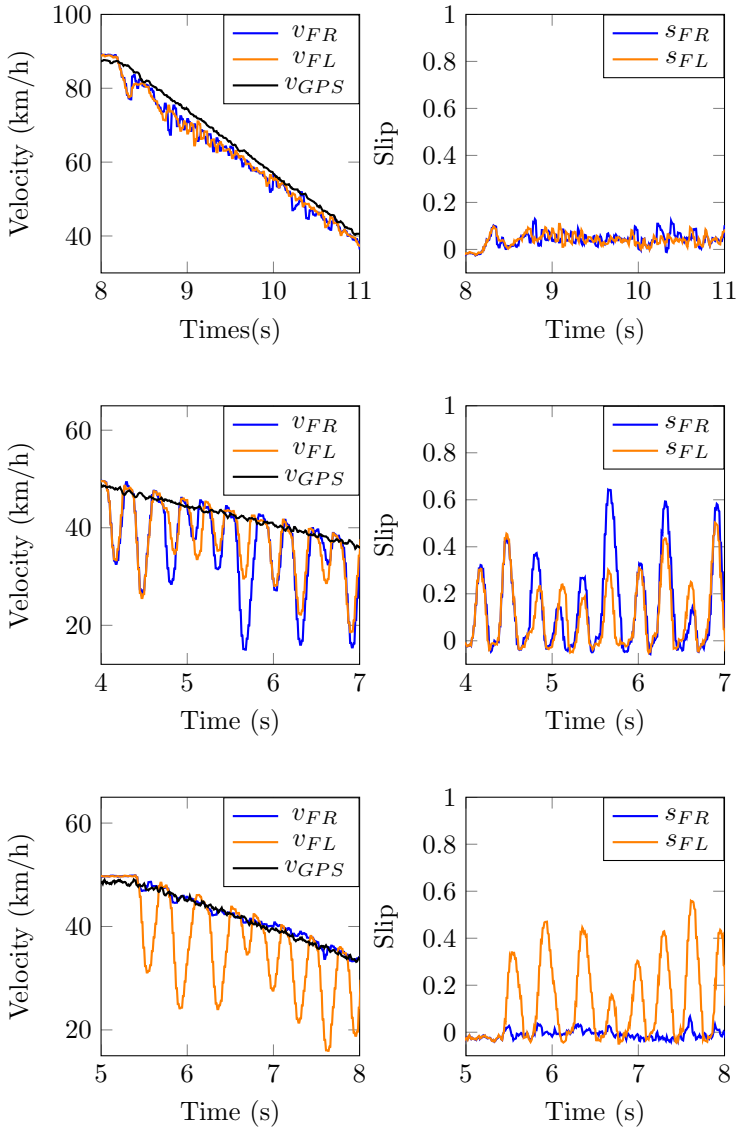

Figure 3.1: *The figure shows the behavior during three different braking situations. With the measured wheel and GPS velocities in the left plots and the corresponding slip values to the right. The top plots shows a high-μ braking, the middle plots shows a low-μ braking and the bottom plots shows a μ-split braking.*

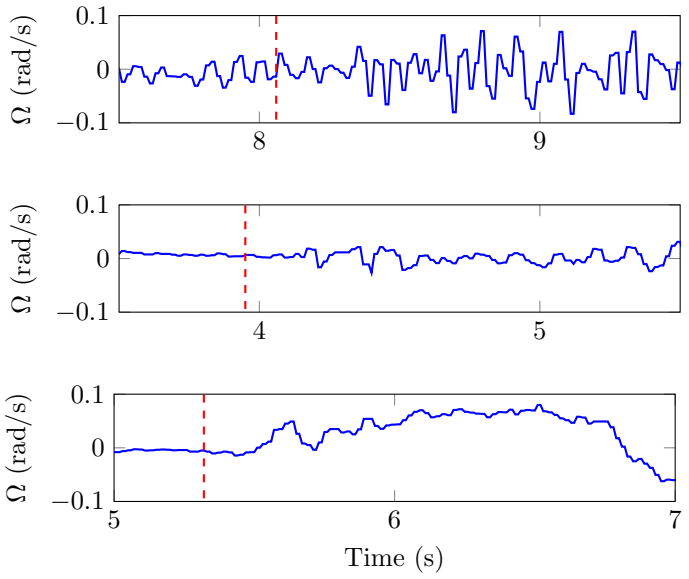

Figure 3.2: *The figure shows the measured yaw rate for three different braking situations. The upper plot shows a high-μ braking, the middle plot shows a low-μ braking and the lower plot shows a μ-split braking. The red line shows where the braking starts.*

3.2.1 Additional Logic

Since the detector only compares the difference in slip there are some situations that will be hard to distinguish from a μ-split situation. This can be seen in the low-μ situation in Fig. 3.1. The overall behavior in the figure is easy to distinguish from the μ-split situation in the same figure. During some parts of the low-μ braking there is a big difference in slip between the left and right wheel, this could lead to false detection.

To solve this problem the detector has a certain time limit from the moment the braking begins to detect a μ-split situation. After this time limit the detection algorithm is changed to increase the robustness of the detector. This additional logic uses the typical μ-split behavior, seen in Fig. 3.1, by the use of two slip limits, a lower and a upper. To detect a μ-split situation the lower of the two slips must remain under the lower limit, while the higher of the two slips needs to pass the upper limit at two separate occasions within a certain time interval Δt. As seen in Fig. 3.1, during high-μ braking the slip is below 0.15. This is set as the lower limit in the additional logic and the upper limit is a tuning parameter.

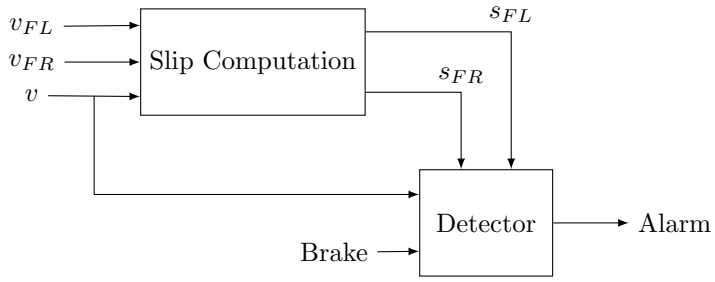

Figure 3.3: *Block diagram of the kinematic detector.*

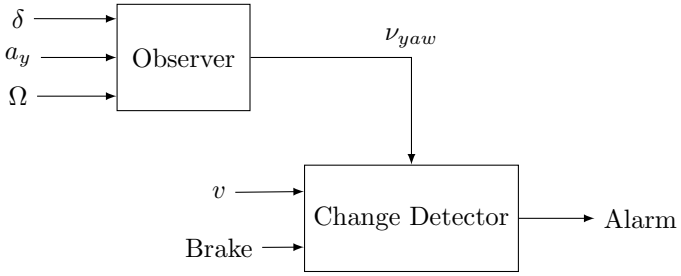

Figure 3.4: *Block diagram of the dynamic detector.*

3.3 Dynamic Detector

The dynamic detector uses a vehicle model and an observer to estimate the unexpected yaw torque during a μ-split braking situation. The unexpected signal is then sent to a change detection algorithm that is used to set an alarm. The change detector is only active during braking and when the velocity is above 20 km/h due to the same reasons discussed in Sec. 3.2. In Fig. 3.4 a overview of the system with its signals is shown.

3.3.1 Sliding Mode Observer

The SMO from Sec. 2.2.1 is used in the dynamic μ-split detector. The observer is based on the single-track model (2.2) that also includes an unexpected force, F_{un}, and an unexpected yaw torque, M_{un}, as disturbances. Where M_{un} is the yaw torque from the brake system. The state space model used in the SMO has the form

$$\begin{aligned} \dot{\bar{x}} &= A\bar{x} + B\bar{u} + F\begin{bmatrix} F_{un} \\ \dot{F}_{un} \\ M_{un} \end{bmatrix} \\ \bar{y} &= C\bar{x} \quad \text{and} \quad \bar{u} = \begin{bmatrix} \delta \\ \dot{\delta} \end{bmatrix} \end{aligned} \tag{3.1}$$

The complete derivation and matrix values can be seen in App. A.1. The final observer with the error injection signals ν_{acc} and ν_{yaw} becomes

$$\begin{aligned} \dot{\hat{x}} &= A\hat{x} + B\bar{u} + \begin{bmatrix} \nu_{acc} \\ \nu_{yaw} \end{bmatrix} \\ \begin{bmatrix} \nu_{acc} \\ \nu_{yaw} \end{bmatrix} &= \begin{bmatrix} \rho_{acc} \\ \rho_{yaw} \end{bmatrix} \text{sign}(\bar{y} - C\hat{x}) \end{aligned} \tag{3.2}$$

where ρ_{acc} and ρ_{yaw} are the observer gains and these are tuning parameters. The error injection signals are computed from the measurement errors and contains information about the unexpected signals F_{un} and M_{un}. In [5] it is shown that the error injection signal ν_{yaw} is dominated by the unexpected yaw torque. The injection signal during a high-μ braking can be seen in Fig. 3.5. The upper plot shows the signal with good tuning on ρ_{yaw}, where it can be seen that sliding has been obtained. The middle plot shows the signal with too low tuning on ρ_{yaw}. The low tuning does not make $\hat{x}$ track the measured signal perfectly and therefore sliding has not occurred. The bottom plot show the signal with too high tuning on ρ_{yaw}. The injection signal will then always overcompensate giving the spiky behavior. The reason that good tuning is needed is because the signal ν_{yaw} will be low passed filtered and then used to detect a μ-split braking. In Fig. 3.6 the low passed signals from Fig. 3.5 are shown. The plots in Fig. 3.6 shows what will happen with insufficient tuning. The signal shows a braking situation on a high-μ surface, where the braking starts after 8.06 s. The upper plot with good tuning seems to still maintain sliding and does not show any significant reactions. The middle plot with to low tuning have a clear reaction that would give a false alarm. The bottom plot shows a to high tuning and the signal is not good enough to use for detection.

3.3.2 Change Detection

It is not possible to use a fixed threshold on the signals used for detection. This is because model errors and measurement noise will be seen in the injection signals. In Fig. 3.7 it can be seen that it is hard to set a fixed limit without having false detections. Both the low-μ braking and the μ-split braking have noise with spikes. But in the μ-split plot it can be seen that during braking there is a change in the mean value of the signal. This is the change caused by the unexpected yaw torque.

To be able to detect the change a CUSUM algorithm is used on the low pass filtered error injection signal. There are two design parameters to tune: ϕ and the threshold, $limit$. These are tuned based on test cases with braking on high-μ surfaces, low-μ surfaces and μ-split surfaces. The algorithm in (2.18) is changed to the two-sided algorithm

$$\begin{aligned} T_{pos,k} &= max\{0, T_{pos,k-1} + r_k - \phi\} \\ T_{neg,k} &= min\{0, T_{neg,k-1} + r_k + \phi\} \end{aligned} \tag{3.3}$$

The two sided algorithm makes it possible to detect rotation in both directions.

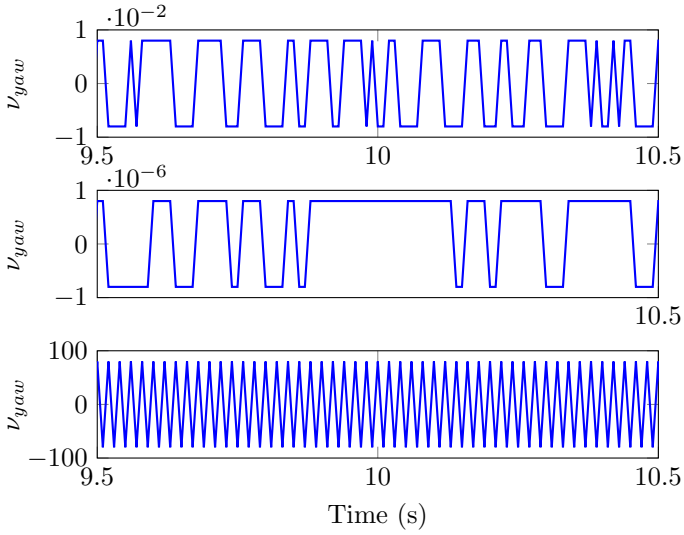

Figure 3.5: *The figure shows the error injection signal for three different tunings on ρ_{yaw}. The upper plot has a good tuning, the middle plot has too low tuning and the lower plot has too high tuning.*

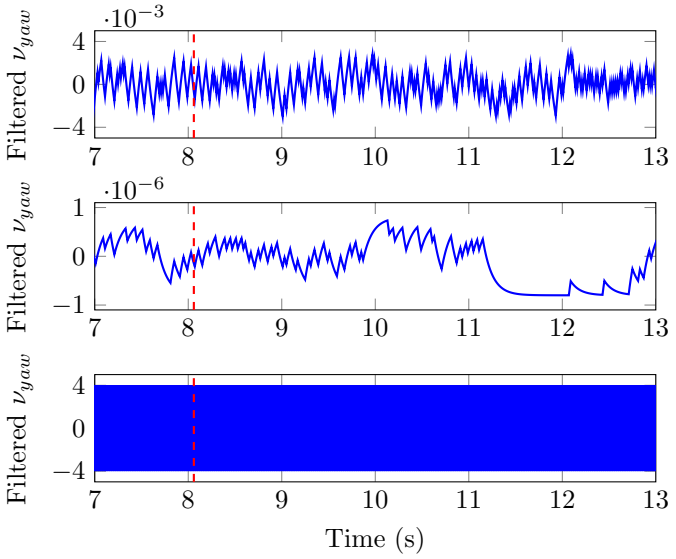

Figure 3.6: *The figure shows the low passed filtered error injection signal for three different tunings on ρ_{yaw}. The upper plot has a good tuning, the middle plot one has to low tuning and the lower plot has to high tuning. The red line indicates where the braking starts.*

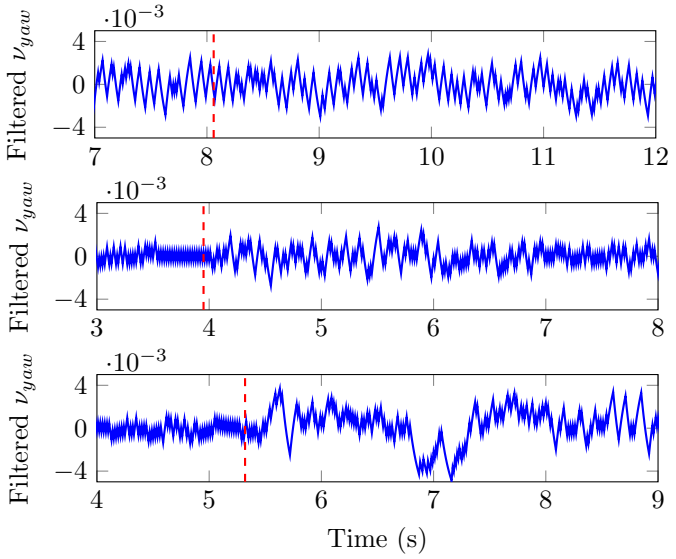

Figure 3.7: *The figure shows the filtered error injection signal for three different braking situations. The upper plot shows a braking on a high-μ surface, the middle on a low-μ surface and the lower on a μ-split surface. The red line indicates where the braking starts.*

4

Simulation Environment for Controller Development

The main purpose of the simulation environment is not to perfectly represent a real vehicle during driving. Instead the purpose is to replicate the behavior during a μ-split braking where the difference in the longitudinal force should generate a yaw torque on the vehicle. The simulation environment is developed in sub models making it easy to replace or change individual parts of the model.

4.1 Vehicle Dynamic Model

In order to simulate the motion of a tractor during μ-split braking a vehicle model is needed. The vehicle model is presented in this section.

4.1.1 Longitudinal and Lateral Dynamics

The longitudinal and lateral dynamics in the model are based on (2.5). With the addition of the air resistance from (2.6) in the longitudinal equation. This is done since the air resistance has an impact on the longitudinal deceleration especially

during high velocities. The equation of motion becomes

$$\begin{aligned} m(\dot{v}_x - v_y\Omega) =& F_{xFL}\cos(\delta) + F_{xFR}\cos(\delta) - F_{yFL}\sin(\delta) \\ & - F_{yFR}\sin(\delta) + F_{xFL} + F_{xFR} + F_D \\ m(\dot{v}_y + v_x\Omega) =& F_{xFL}\sin(\delta) + F_{xFR}\sin(\delta) + F_{yFL}\cos(\delta) \\ & + F_{yFR}\cos(\delta) + F_{yRL} + F_{y,RR} \\ I_z\Omega =& (F_{x,FR}\cos(\delta) - F_{xFL}\cos(\delta) + F_{xRR} \\ & - F_{xRL} + F_{yFL}\sin(\delta) - F_{yFR}\sin(\delta))l_t \\ & + (F_{xFL}\sin(\delta) + F_{xFR}\sin(\delta) + F_{yFL}\cos(\delta) + F_{yFR}\cos(\delta))l_f \\ & - (F_{yRL} + F_{yRR})l_r \\ F_D =& \frac{1}{2}C_D\rho A v^2 \end{aligned} \tag{4.1}$$

The reason that the four wheel model is used instead of the single-track model is that a μ-split situation can be created using the different longitudinal force on the left and right side of the vehicle.

4.1.2 Vertical Dynamics

During μ-split braking both longitudinal and lateral load transfer will occur. Since the lateral acceleration during this situation is relatively small, the lateral load transfer will not be considered in the model. The longitudinal load transfer is modeled using (2.7). The normal force computed for the front and rear axle is then split equally between the tires on the corresponding axle resulting in

$$\begin{aligned} F_{z,i} &= \frac{1}{2}mg\left(\frac{l_r}{l_r + l_f} - \frac{ah}{g(l_f + l_r)}\right) \\ F_{z,j} &= \frac{1}{2}mg\left(\frac{l_f}{l_r + l_f} + \frac{ah}{g(l_f + l_r)}\right) \end{aligned} \tag{4.2}$$

where $i = FL, FR$ and $j = RL, RR$.

4.1.3 Tire Force

The total longitudinal force in the simulation is used as input to the simulation environment. The lateral force are computed based on the motion of the vehicle.

Longitudinal Force

The longitudinal force is used as input to the simulation and is computed using

$$F_x = \eta m a_d \tag{4.3}$$

where m is the vehicle mass, η is a tuning parameter and a_d is the desired acceleration. The desired acceleration will be set according the measurements from real world braking tests. The tuning parameter η is used to get a more accurate

simulation compared to measurements. A good value on η is 1.15 and this value gave the results in Sec. 4.2.

The longitudinal force is distributed between the front and rear axle with the same proportions as the normal force distribution. The distribution is computed as

$$\begin{aligned} \frac{K_{bf}}{K_{br}} &= \frac{l_r - \frac{a}{g}h}{l_f + \frac{a}{h}h} \\ K_{bf} + K_{br} &= 1 \end{aligned} \tag{4.4}$$

where K_{bf} and K_{br} are the parts of the total longitudinal force applied to the front and rear axle. The μ-split situation is achieved by distributing the longitudinal force unevenly between the left and right side of the vehicle based on the friction. The distribution is done using

$$\begin{aligned} F_{x,FL} &= K_{bf} F_x \frac{\mu_L}{\mu_L + \mu_R} \\ F_{x,FR} &= K_{bf} F_x \frac{\mu_R}{\mu_L + \mu_R} \\ F_{x,RL} &= K_{br} F_x \frac{\mu_L}{\mu_L + \mu_R} \\ F_{x,RR} &= K_{br} F_x \frac{\mu_R}{\mu_L + \mu_R} \end{aligned} \tag{4.5}$$

Lateral Force

The lateral forces computed in the simulation model are based on the linear cornering stiffness from (2.10) where the force is scaled with the friction coefficient resulting in

$$\begin{aligned} F_{y,FL} &= C_\alpha \alpha_{FL} \mu_L \\ F_{y,FR} &= C_\alpha \alpha_{FR} \mu_R \\ F_{y,RL} &= C_\alpha \alpha_{RL} \mu_L \\ F_{y,RR} &= C_\alpha \alpha_{RR} \mu_R \end{aligned} \tag{4.6}$$

By using this model there is no possibility for the tire to reach saturation. This problem is solved by computing the maximum contact force the tire can deliver by using (2.8). In the simulation environment the maximum lateral and longitudinal force the tires can deliver are assumed to be equal. The friction ellipse in (2.12) can therefore be rewritten as

$$F_{x,i}^2 + F_{y,i}^2 \leq (\mu F_{z,i})^2 \tag{4.7}$$

where $i = FL, FR, RL, RR$. The maximum available lateral force for each wheel is then calculated with

$$F_{y,max,i} = \sqrt{(\mu F_{z,i})^2 - F_{x,i}^2} \tag{4.8}$$

where $i = FL, FR, RL, RR$.

Table 4.1: *The table shows the model parameters used in the simulation environment.*

Name	Notation	Value	Unit
Front Axle to CoG	l_f	2.5	[m]
Rear Axle to CoG	l_r	2.5	[m]
Track width	l_t	1	[m]
CoG Height above Ground	h	1.5	[m]
Moment of Inertia	I_z	44000	[kgm^2]
Vehicle Mass	m	15000	[kg]
Drag Coefficient	C_d	0.7	[-]
Frontal Area	A	7.5	[m^2]
Air Density	ρ	1.225	[kg/m^3]
Cornering Stiffness	C_α	262500	[N/rad]

4.1.4 Model Parameters

There are several parameters in the model that needs to be determined. Some of the parameters are difficult to approximate, such as the cornering stiffness, while others such as the mass are easier. All parameters used can be seen in the Tab. 4.1.

4.1.5 Global Position

An autonomous vehicle will follow a given path. In order to do this the vehicle needs information about its position. This is usually done by fusing information from different sensors. Instead of modeling the sensor fusion it is assumed that the vehicle position in the global coordinate system is known. When the vehicle moves the body coordinate system of the vehicle will no longer be oriented in the same direction as the global coordinate system as seen in Fig. 4.1. The global position of the vehicle can be computed as

$$\begin{bmatrix} X \\ Y \\ \theta \end{bmatrix} = \int \begin{bmatrix} \cos(\theta) & -\sin(\theta) & 0 \\ \sin(\theta) & \cos(\theta) & 0 \\ 0 & 0 & 1 \end{bmatrix} \begin{bmatrix} v_x \\ v_y \\ \Omega \end{bmatrix} \mathrm{d}t \tag{4.9}$$

where X and Y are the global coordinates and θ is the current heading of the vehicle which is the same as the orientation of the local coordinate system.

4.2 Validation of Simulation Environment

The simulation environment is validated by comparing it to measured data from real tests. The tests are from a test track with several turns and test of μ-split braking. To be able to simulate the model in the same scenarios the input has to be determined. There are two inputs that has to be set, the steering angle and the total longitudinal force.

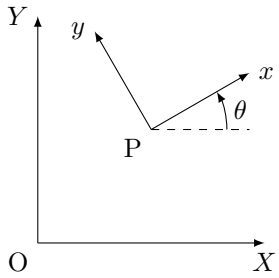

Figure 4.1: *The figure shows the global coordinate system X and Y with the vehicle body coordinate system x and y. θ is the angle between the body- and global coordinate system and P is the position of the vehicle in the global coordinate system.*

The steering angle can be obtained from the measurements directly. The longitudinal force has to be computed using (4.3) where a_d comes from the measurements. A simulation with these inputs are then compared to the measurements, the interesting signals are yaw rate and longitudinal velocity. The reason these signals are considered is that they are the most important signals when describing a μ-split braking situation.

4.2.1 Normal Driving

To validate the simulation environment it is tested with the same input forces and steering angles as a normal driving case. The left and right friction coefficient are set to the same value. This gives an even distribution between the left and the right side according to (4.5), where $\mu_L = \mu_R = 0.8$. The longitudinal force used as input is distributed according to (4.4) and (4.5), where the resulting force at each wheel can be seen in Fig. 4.2. The driving was performed at quite high velocities as can be seen in Fig. 4.3. The steering seen in the lower plot of Fig. 4.4 is quite aggressive considering the velocity where there are big steering angles during the turns.

As seen in Fig. 4.3 the simulation describes the longitudinal dynamics with good accuracy. The error is small during the entire simulation and it is able to follow the accelerations and decelerations, but it can be seen that the simulation has a slightly higher acceleration and deceleration compared to the measured data. Resulting in that the error changes during these phases. A growing trend throughout the simulation time can be seen in the error plot. This probably depends on the uncertainties in the computed input force. However, the trend is quite small and the error remains at a small level throughout the simulation. A μ-split braking will not last for 75 s therefore the trend will be negligible.

In Fig. 4.4 the simulated yaw rate and the measured yaw rate are shown. It can clearly be seen that the simulated signal tracks the measured signal with high accuracy and with small errors as seen in the middle plot. These small errors may

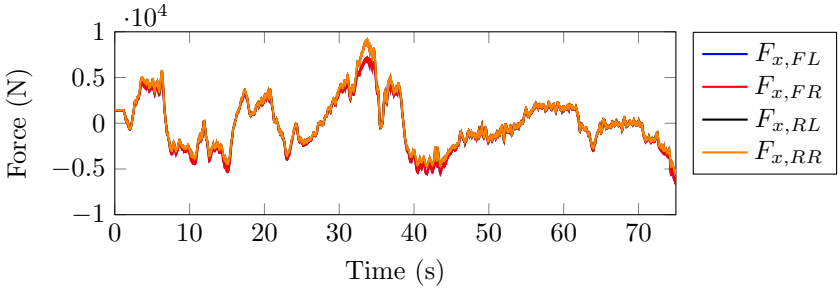

Figure 4.2: *The figure shows the longitudinal forces during normal driving. The input to the simulation is the sum of all forces.*

be explained by uncertainties in the modeled parameters such as the cornering stiffness of the tires, C_α, and the moment of inertia, I_z.

4.2.2 Braking During µ-split

The longitudinal force is distributed between the left and right hand side according to (4.5). Since the friction coefficients from the test are unknown they are assumed to $\mu_L = 0.8$ and $\mu_R = 0.2$ since these are common values for the test surfaces, asphalt and ice. The longitudinal force used as input is distributed according to (4.4) and (4.5), where the resulting force at each wheel can be seen in Fig. 4.5. The model describes the longitudinal velocity well as seen in Fig 4.6, with no drift as could be seen in Sec. 4.2.1. During the braking the deceleration achieved in the simulation is very similar to the one in the real test, which indicates a well performing model. In Fig 4.7 the measured yaw rate, the simulated yaw rate and the steering angle can be seen. When the braking begins there is an evident reaction in the simulated yaw rate similar to the one measured. From the comparison in measured and simulated yaw rate and the steering angle it is clear that the simulation reacts quicker to changes in steering angle than the real system.

By looking at Fig. 4.8, 4.9 and 4.10 a simulation with lower initial velocity, 50 km/h, is compared to a measured file. As seen in Fig. 4.9 the simulation replicates the velocity as good as in Fig. 4.6. Noticeable is that the yaw rate seems to be more accurate at a lower initial velocity if compared to Fig. 4.7. This could be explained by the smaller steering angles and that the dynamics are more damped and stable during lower velocities.

The conclusion that can be drawn from the simulation validation is that the simulation environment works better during normal driving conditions when comparing the simulated and measured yaw rate. The reason the model works better for normal driving than it does for a μ-split braking is that the braking situation include dynamics that are not modeled. When comparing the simulated and measured velocities the simulation environment works better during μ-split braking.

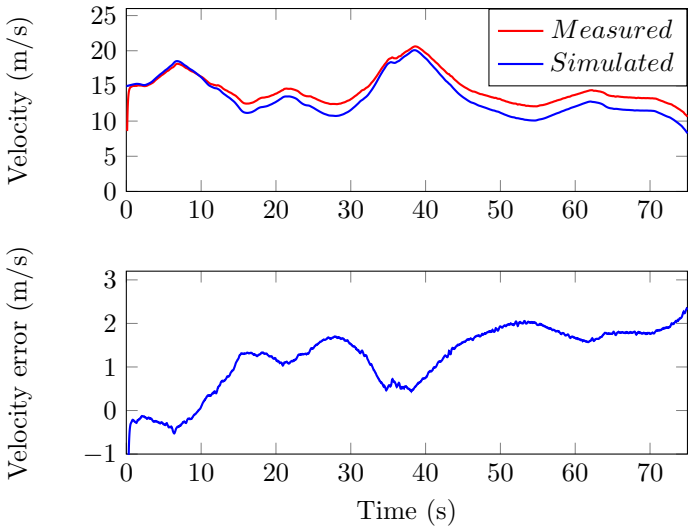

Figure 4.3: *The figure shows signals during normal driving. The upper plot shows the measured and simulated longitudinal velocities. The lower plot shows the difference between these signals.*

This could be explained by the uncertainty in the computed longitudinal force which seems to be greater during normal driving compared to braking. The simulation environments weaknesses can be broken down to three different parts, uncertainties of the friction coefficient, a simplified tire model and the functionality of the brake system.

Friction Coefficient At the test track where the measurements were taken, the braking was done with a split between asphalt and wet plastic with similar properties as ice. The exact μ values from the test are not known. Therefore they are approximated to common values for the respective surface: 0.8 for asphalt and 0.2 for ice. In the simulation the friction coefficients are constant, while in reality they most likely vary along the test track.

Tire model The tire model used in the simulation is simple. The lateral force is assumed to be proportional to the slip angle until it saturates when reaching its limitation, computed with (2.12). This model does not consider that the lateral force decrease when sliding begins. The dependency of the friction coefficient is also simplified, where μ is used to scale the lateral force as done in (4.6) when in reality it changes the behavior of the slip angle-lateral force curve.

Brake system During a μ-split situation the brake system adjusts the brake pressure to maintain stability and maximize the brake force. This leads to variations in the brake force distribution throughout the braking. In the simulation

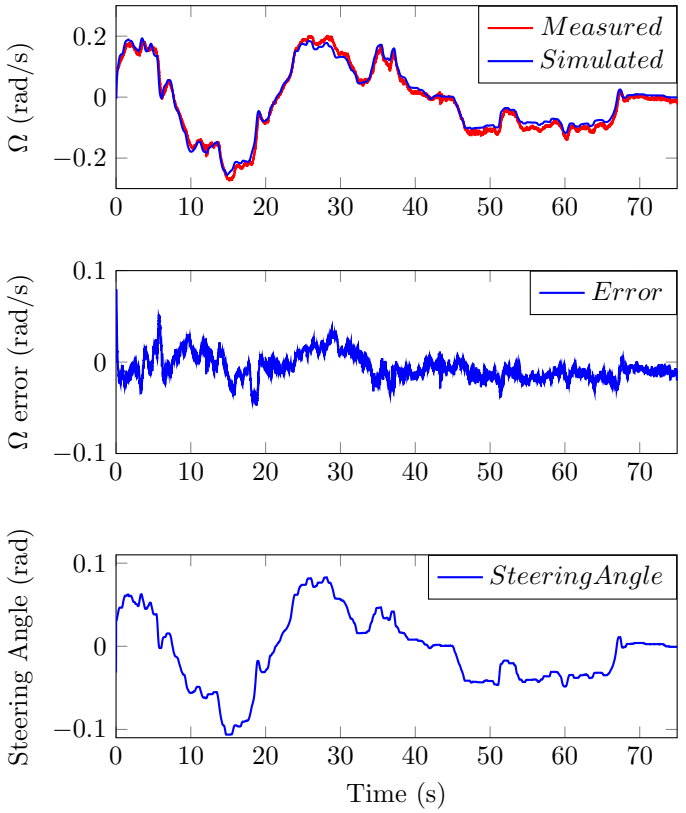

Figure 4.4: *The figure shows signals during normal driving. The upper plot shows the measured and simulated yaw rate, the middle plot shows the difference between these signals and the lower plot shows the steering angle.*

environment this is not considered, for example the ABS is not modeled. Instead the brake force computed from the measured deceleration is distributed between the left and right side based on the estimated μ-value. The brake force distribution remains constant through the entire simulation.

The combination of these different parts lead to uncertainties of how the forces are distributed between the different tires during the μ-split braking. It also leads to uncertainties of the amount of force each tire can be subjected to before saturation occurs. This can explain why the initial peak in yaw rate is lower in the simulation compared to the measurement. With a given steering angle the tire should be able to produce a certain amount of lateral force, given that the tire does not reach saturation. Which in the measured case most likely has happened. The measured yaw rate continues to increase and does not start to decrease until the force distribution changes and the tire is able to produce the desired lateral

force. This can also explain why the simulation reacts quicker to changes in steering angle compared to the real system.

4.2.3 Model Reliability

The model has shown good behavior during normal driving which strengthens the reliability. However, for the μ-split braking situation the results have not been as good in terms of yaw rate, as discussed earlier. Even though the model does not capture the situation perfectly, the most important behavior during a μ-split braking, the initial peak in yaw rate, is captured in a good way. It should also be noticed that the choice of the longitudinal force as input and to distribute the longitudinal force to the different sides is a good method for creating a μ-split situation. Even though the size of the signals is not perfect the overall behavior is sufficient enough to investigate and compare different controllers with each other.

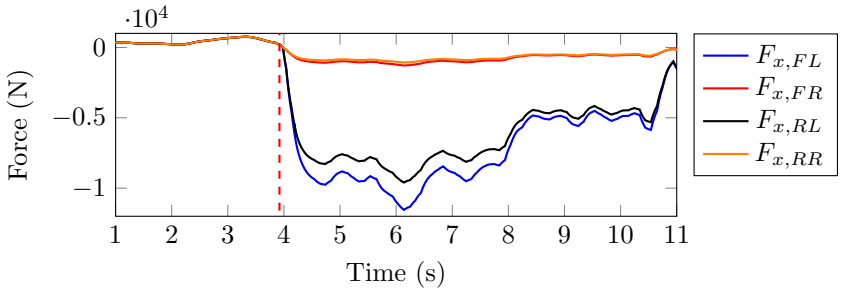

Figure 4.5: *The figure shows the longitudinal forces from a μ-split braking with initial velocity of 70 km/h. The input to the simulation is the sum of all forces.*

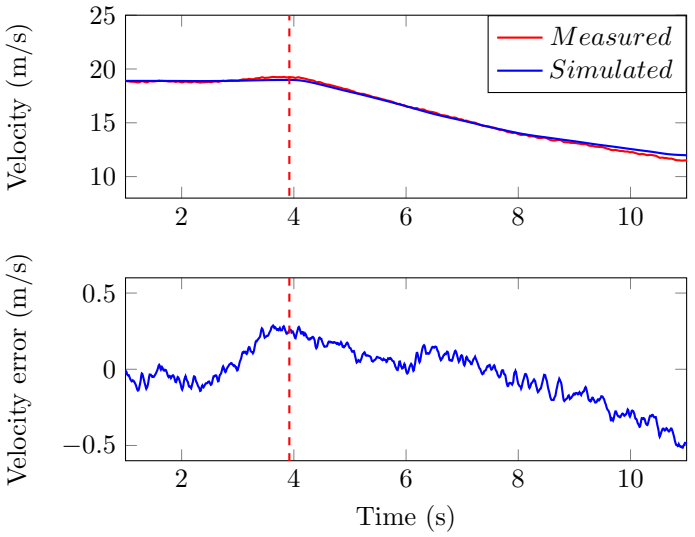

Figure 4.6: *The figure shows signals from a μ-split braking with a initial velocity of 70 km/h. The upper plot shows the measured and simulated velocity. The lower plot shows the difference between these signals.*

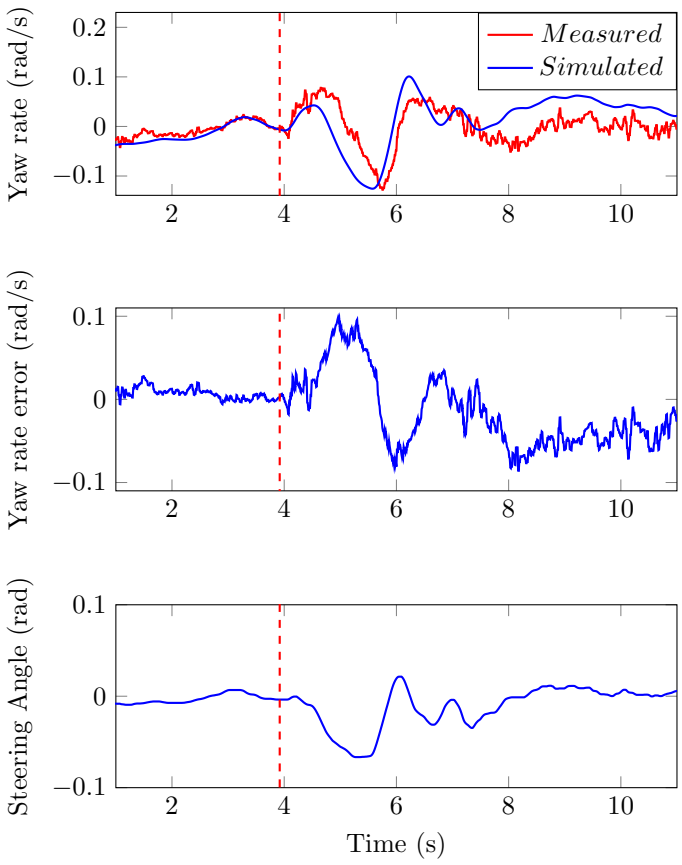

Figure 4.7: *The figure shows signals from a μ-split braking with a initial velocity of 70 km/h. The upper plot shows the measured and simulated yaw rate, the middle plot shows the difference between these signals and the lower plot shows the steering angle.*

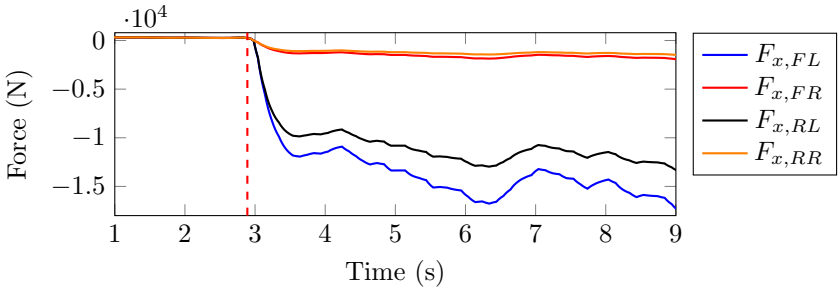

Figure 4.8: *The figure shows the longitudinal forces from a μ-split braking with initial velocity of 50 km/h. The input to the simulation is the sum of all forces.*

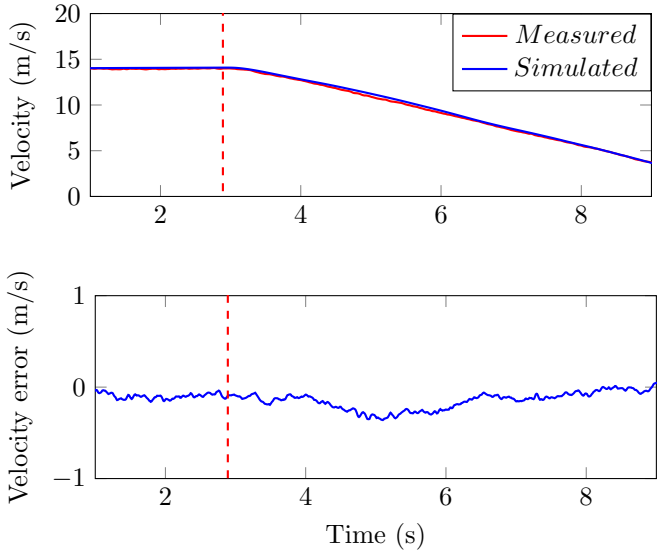

Figure 4.9: *The figure shows signals from a μ-split braking with a initial velocity of 50 km/h. The upper plot shows the measured and simulated velocity. The lower plot shows the difference between these signals.*

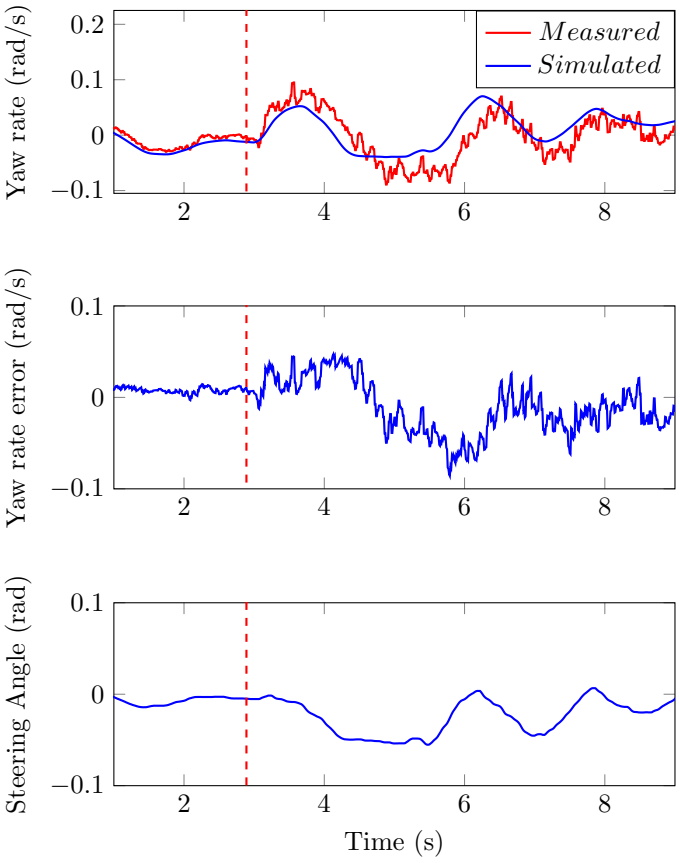

Figure 4.10: *The figure shows signals from a μ-split braking with a initial velocity of 50 km/h. The upper plot shows the measured and simulated yaw rate, the middle plot shows the difference between these signals and the lower plot shows the steering angle.*

5
Steering Control

This chapter will present an analysis of the desired steering behavior during a μ-split braking. The proposed control methods that could be used in an autonomous tractor are also presented. The main purpose for the lateral control in an autonomous vehicle is to follow a given path. A μ-split braking is a situation where the dynamic behavior of the vehicle has a significant role. By assuming that a μ-split situation is possible to detect it is investigated how the control strategy can be changed to increase the performance. To do this the first approach is to have a different tuning on the kinematic path follower. The second approach is to add a dynamic controller on top of the path follower. The reason that the dynamic controller is not included in the path follower is to have them independent of each other to make the system more modular.

5.1 Steering Behavior During µ-split Braking

In this section the desired steering behavior during a μ-split braking situation will be investigated from three point of views: vehicle dynamics, kinematic path errors and a driver.

5.1.1 Vehicle Dynamics

The single track model in (2.2) with an additional torque, M_{un}, generated from the μ-split braking situation together with (2.9) and (2.3) can be written as

$$\begin{aligned}
\dot{v}_y &= \overbrace{-\frac{2C_{\alpha f}+2C_{\alpha r}}{mv_x}}^{a_1} v_y \overbrace{-\left(v_x+\frac{2l_fC_{\alpha f}-2l_rC_{\alpha r}}{mv_x}\right)}^{a_2}\Omega+\overbrace{\frac{2C_{\alpha f}}{m}}^{b_1}\delta \\
\dot{\Omega} &= \underbrace{-\frac{2l_fC_{\alpha f}-2l_rC_{\alpha r}}{I_zv_x}}_{a_3} v_y \underbrace{-\frac{2l_f^2C_{\alpha f}+2l_r^2C_{\alpha r}}{I_zv_x}}_{a_4}\Omega+\underbrace{\frac{2l_fC_{\alpha f}}{m}}_{b_2}\delta \underbrace{-\frac{1}{I_z}}_{e_1} M_{un}
\end{aligned} \tag{5.1}$$

In matrix form this becomes

$$\begin{bmatrix}\dot{v}_y\\ \dot{\Omega}\end{bmatrix}=\begin{bmatrix}a_1 & a_2\\ a_3 & a_4\end{bmatrix}\begin{bmatrix}v_y\\ \Omega\end{bmatrix}+\begin{bmatrix}b_1\\ b_2\end{bmatrix}\delta+\begin{bmatrix}0\\ e_1\end{bmatrix}M_{un} \tag{5.2}$$

With the assumption that zero yaw rate is wanted during a straight line braking. The steady state equations can be written as

$$\begin{bmatrix}0\\ 0\end{bmatrix}=\begin{bmatrix}a_1 & a_2\\ a_3 & a_4\end{bmatrix}\begin{bmatrix}v_{y,ss}\\ 0\end{bmatrix}+\begin{bmatrix}b_1\\ b_2\end{bmatrix}\delta_{ss}+\begin{bmatrix}0\\ e_1\end{bmatrix}M_{un} \tag{5.3}$$

By solving for v_y and δ the following results are obtained

$$\begin{bmatrix}v_{y,ss}\\ \delta_{ss}\end{bmatrix}=-\begin{bmatrix}a_1 & b_1\\ a_3 & b_2\end{bmatrix}^{-1}\begin{bmatrix}0\\ e_2\end{bmatrix}M_{un}=\frac{e_1}{a_1b_2-a_3b_1}\begin{bmatrix}-b_1\\ a_1\end{bmatrix}M_{un} \tag{5.4}$$

In these equations it is possible to see that a steady state behavior during a μ split situation does not have δ and v_y equal to zero instead they will depend on M_{un}. By substitute back to the original parameters the following expressions appear

$$\begin{cases} v_{y,ss} &= -\frac{v_x}{2C_{\alpha r}(l_f+l_r)}M_{un}\\ \delta_{ss} &= -\frac{C_{\alpha f}+C_{\alpha r}}{2C_{\alpha f}C_{\alpha r}(l_f+l_r)}M_{un}\end{cases} \tag{5.5}$$

Note that the expressions for $v_{y,ss}$ in (5.5) depends on v_x and will change over time. However, the expression for δ_{ss} will not change over time and the steady state behavior is to keep a constant steering angle throughout the braking. By using the body slip definition as in (2.4) and the lateral velocity from (5.5) the following expression for body slip is obtained

$$\beta_{ss}=\arctan\left(\frac{-M_{un}}{2C_{\alpha r}(l_f+l_r)}\right) \tag{5.6}$$

This expression does not have any parameters that change over time and therefore the body slip will be constant throughout the braking. The steady state behavior during a μ-split braking situation will be to drive with a constant steering angle as seen in (5.5) and a constant body slip angle as seen in (5.6). Note that the amount of steering and body slip during steady state depends on the amount of unexpected yaw torque, M_{un}.

5.1.2 Kinematic Path Errors

The goal during path following is to have zero lateral deviation and zero heading error compared to a given path. The kinematic error dynamics are given by (2.1) and does not give the possibility to include a unwanted torque. These are non-linear and can be linearized. This is done by first calculating the Jacobian matrix as

$$\frac{\partial}{\partial x} = v \begin{bmatrix} 0 & \cos(\theta_e) \\ -\frac{c(s)\cos(\theta_e)}{(1-dc(s))^2} & \frac{\sin(\theta_e)}{1-dc(s)} \end{bmatrix} \tag{5.7}$$

$$\frac{\partial}{\partial u} = v \begin{bmatrix} 0 \\ 1 \end{bmatrix} \tag{5.8}$$

By doing the linearization around zero for both states and assuming a straight road $c(s) = 0$, the path following problem can be written as

$$\underbrace{\begin{bmatrix} \dot{d} \\ \dot{\theta} \end{bmatrix}}_{=0} = \begin{bmatrix} 0 & v \\ 0 & 0 \end{bmatrix} \begin{bmatrix} d \\ \theta \end{bmatrix} + \begin{bmatrix} 0 \\ v \end{bmatrix} u \tag{5.9}$$

During steady state all derivatives are equal to zero and this gives two equations

$$\begin{cases} v\theta_{ss} = 0 \\ v u_{ss} = 0 \end{cases} \tag{5.10}$$

By assuming that $v \neq 0$ then θ_{ss} and u_{ss} has to be zero.

$$u_{ss} = 0 \Rightarrow \frac{1}{l_f + l_r} \tan \delta_{ss} = 0 \Rightarrow \delta_{ss} = 0 \tag{5.11}$$

The resulting steady state kinematic path errors are equal to zero which is expected. Since a path follower based on the kinematic path errors does not consider the vehicle dynamics, it will not be able to converge both the heading error and lateral error to zero during a μ-split situation. The consequences of this will be investigated in Sec. 6.2.

5.1.3 Driver Behavior

In Fig. 5.1 a drivers reaction to a μ split behavior can be seen. The upper plot shows the wheel angle, δ and the negative heading error, θ. In this case the heading error comes from integrating the yaw rate from the start of the braking. The lower plot shows the corresponding negative yaw rate and steering angular velocity. The reason that the negative heading angle and yaw rate is shown is that it will be easier for comparison. As seen in the plot the driver reacts to a heading error and tries to compensate for it with the same amount of steering angle as heading error. After a short period of time the driver however turns the wheels more such that they start pointing towards the path. This is intuitive since the

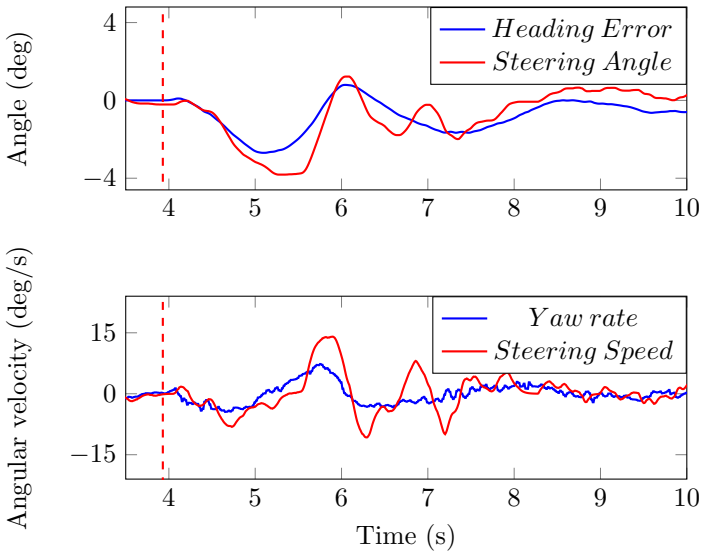

Figure 5.1: *The figure shows a drivers response to a μ-split braking situation with the an initial velocity of 70 km/h and high-μ at the left hand side. The upper plot shows the negative heading error and the wheel angle. The lower plot shows the negative yaw rate and the steering angular velocity. The dotted line indicates the start of the braking.*

driver wants to have the same vehicle heading as the path. However as the second plot shows the initial peak in yaw rate will be compensated for and the yaw rate will return to zero, this happens right after five seconds. It can be seen that the driver keeps the same steering angle for a short period, even as the heading error starts to decrease. This results in a high change in the yaw rate towards the low-μ side. This delay leads to a fast correction is needed as can be seen in the second plot, where there is a peak in the steering speed. After this the steering angle changes at a higher frequency than the heading error. This indicates that it is difficult to keep stability and at the same time keep the heading.

5.1.4 Comparison Between Vehicle Dynamics, Kinematic Path Error and Driver Behavior

As described in Section 5.1.1 and 5.1.2 the wanted steering angle for maintaining lateral stability at a steady state braking and the steering angle for maintaining zero path errors contradict each other. As can be seen in (5.6) the body slip angle will not be equal to zero. During straight line braking the body slip angle and the heading error are equal, assuming that the velocity vector, v, is parallel to the path. If compared to a normal braking where M_{un} in (5.1) is equal to zero, the wanted steering angle and the lateral velocity would be equal to zero. This would not lead to the same contradiction.

The driver seems to have two different goals while steering the vehicle, maintaining lateral stability and keeping zero heading error. At the beginning of the braking the driver notices the unwanted yawing motion and tries to compensate for it to maintain stability. As soon as stability is achieved the driver tries to steer towards the path to maintain the desired heading. After the situation is under control the driver tries to maintain both lateral stability and zero heading error at the same time. This is however hard which is indicated in Fig. 5.1 where it can clearly be seen that the driver has to turn the steering wheel very rapidly until the velocity is decreased and a steadier motion can be performed.

5.2 Path Follower

The path follower (PF) used in this thesis is a LQR, developed from the error dynamics in (5.9). The goal of the PF is to smoothly follow the path while maintaining small errors in heading and lateral deviation. It is difficult to converge the path errors to zero fast while maintaining smooth steering therefore a trade off must be done between these. A simple lane change maneuver is used to tune the controller to the desired behavior. This tuning is used as a benchmark when evaluating the controllers on a μ-split braking. Figure 5.2 shows the controller behavior, the lateral error and the heading error during the lane change maneuver. The controller produces a smooth steering angle and manages to follow the path with small errors.

During μ-split braking the steady state of the vehicle dynamics is to have a non zero steering angle and a non zero body slip angle β as shown in Sec. 5.1.1. Since the body slip angle is assumed to be equal to the heading error as described in Sec. 5.1.4 it is no longer desirable to control the heading error to zero. It is more important to have a small lateral deviation, since it is not possible to achieve both as described in Sec. 2.1.1. A new tuning based on the same PF is developed specifically for the μ-split situation. Due to body slip during steady state the control signal depends more on the lateral deviation. The weighting factor for heading error is decreased and the weighting factor for lateral deviation is increased. This tuning will later be referred to as PFX.

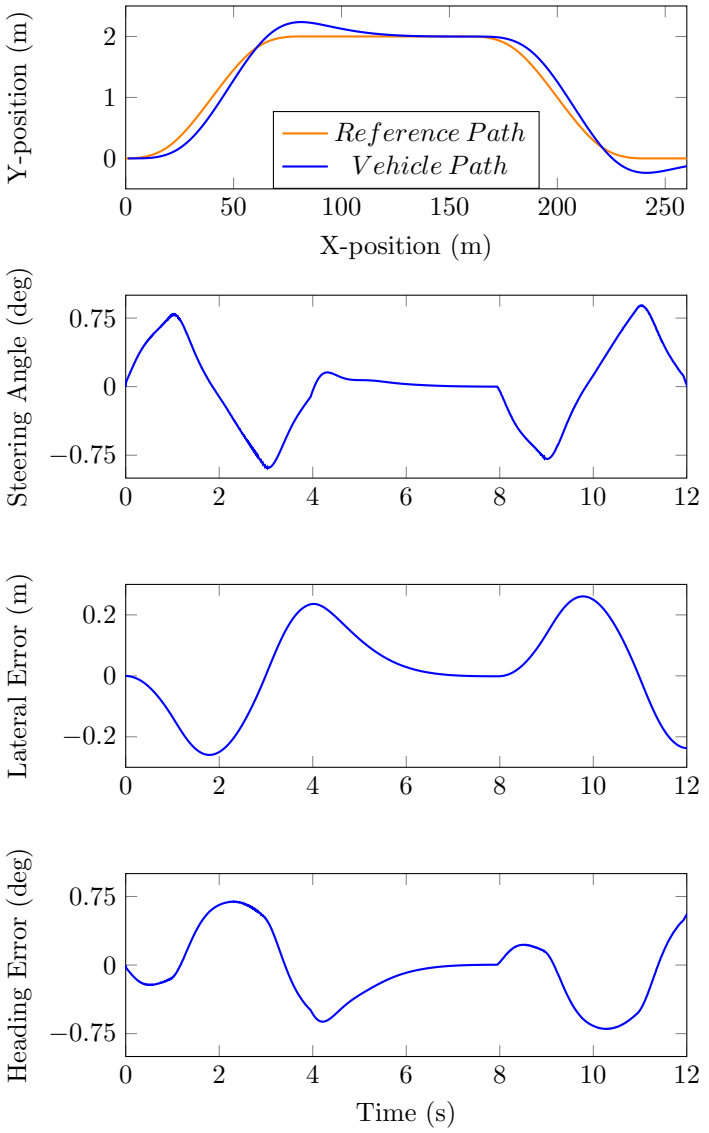

Figure 5.2: *The top plot shows the path used for tuning of the controller and the resulting path from the simulation. The second plot shows the required steering angle during the maneuver. The last two plots shows the lateral deviation and heading error.*

5.3 Path Follower with Active Yaw and Side Drift Control

When a μ-split situation is detected the PF will try to keep the vehicle heading by steering. The steering command can be transformed into a desired yaw rate according to

$$\Omega_{reference} = \frac{v_x}{l_f + l_r} \tan(\delta_{PF}) \tag{5.12}$$

Since there is an unwanted yaw torque the measured yaw rate will be either higher or lower than $\Omega_{reference}$ depending on the steering direction. This is not the wanted behavior and the yaw error can be computed according to

$$\Omega_{error} = \Omega_{reference} - \Omega_{measured} \tag{5.13}$$

This error can be seen as a measure of the disturbance, the unwanted yaw torque, and has to be compensated for. The error can then be transformed into a steering angle by using the inverse of (5.12) resulting in

$$\delta_{yaw} = \arctan\left(\frac{l_f + l_t}{v_x}\Omega_{error}\right) = \arctan\left(\tan(\delta_{PF}) - \frac{l_f + l_r}{v_x}\Omega_{measured}\right) \tag{5.14}$$

Instead of using the kinematic relation in (5.12) to compute δ_{yaw} a simple proportional controller could be used, giving additional tuning possibility.

The other parameter that has to be tracked is the side slip. The reference to the side slip, $\beta_{reference}$, can be set to zero. There are two reasons that the reference is set to zero. The first reason is that a low body slip is desired for lateral stability. The second reason is that the PF tries to control the heading error to zero and as discussed earlier the body slip can be assumed to be equal to the heading error if the vehicle velocity vector is parallel to the path. The body slip is assumed to be estimated in the vehicle then the error can be computed as

$$\beta_{error} = \beta_{reference} - \beta_{measured} \tag{5.15}$$

A simple proportional controller can be used to control the body slip. The resulting controller becomes

$$\delta_{bodyslip} = k_P \beta_{error} \tag{5.16}$$

where k_P is the proportional gain and is tuned to 2.

The total steering angle becomes

$$\begin{aligned} \delta_{tot} &= \delta_{PF} + \delta_{AYC} \\ \delta_{AYC} &= \delta_{yaw} + \delta_{bodyslip} \end{aligned} \tag{5.17}$$

By transforming the path following problem to a lateral stability problem the controller will not only try to follow the path it will also try to stabilize the vehicle. This is a behavior that is more similar to a driver as described in Sec. 5.1.3. This controller will be referred to as Active Yaw Controller (AYC).

5.3.1 Smooth Change After Detection

The AYC will be enabled once a μ-split situation is detected. To ensure a smooth transition the signal is ramped up, the ramp time is set to one second. The reason that one second is used is since it gives a good balance between a smooth behavior and fast correction. This parameter can be tuned to get a faster or a smoother change. The transition is done according to

$$\delta = \delta_{PF} + \alpha\delta_{AYC} \tag{5.18}$$

where α is zero before the detection and then ramps up to one after the detection. The ramp variable α is low pass filtered to get an even smoother transition.

6
Results

The data from a real life test of the detectors are presented as both numerical values and with graphs showing the behavior of the controllers. Data from tests of the proposed controllers in the simulation environment are presented. The controllers where tested on μ-split braking to evaluate the performance. The controllers are compared using both numerical values and graphs.

6.1 Results from µ-Split Detectors

This section presents the results of the real world tests of the μ-split detectors.

6.1.1 Test Environment and Setup

The detectors were tested in a real tractor. The test was performed in a controlled environment on a test track. On the test track it was possible to test low friction braking and μ-split braking. Both of these surfaces were tested to evaluate both performance and robustness of the detectors. For each surface, tests were performed at three different initial velocities: 30 km/h, 50 km/h and 70 km/h. Three tests were performed for each velocity and surface to ensure consistency among the tests.

The tractor used was a 4x2 tractor with a load frame attached to it. This tractor has two axles where the front axle is the steering axle and the rear axle is the driven axle. The load frame made the total weight approximately 15000 kg with approximately the same weight distribution on both the rear and front axle. The tractor was equipped with both ABS and ESP. During the tests the tractor was driven by a test driver that had to compensate for the μ-split situation by steering. It has to be mentioned that the driver knew exactly what was going to happen

Table 6.1: *Test results from μ-split braking with different initial velocities. The number represent the detection time in seconds. A dash indicates a missed detection.*

	Kinematic Detector			Dynamic Detector		
Test	30 km/h	50 km/h	70 km/h	30 km/h	50 km/h	70 km/h
1	0.14	0.08	0.12	-	0.19	0.19
2	0.08	0.10	0.20	0.19	0.18	0.30
3	0.18	0.12	0.22	0.41	0.20	0.33
Avg.	0.13	0.1	0.18	0.3	0.19	0.27

Table 6.2: *Test results from μ-split braking with different initial velocities only using the additional logic. The number represent the detection time in seconds. A dash indicates a missed detection.*

	Additional Logic		
Test	30 km/h	50 km/h	70 km/h
1	0.48	1.31	1.13
2	0.44	0.42	1.36
3	0.44	0.56	0.97
Avg.	0.45	0.76	1.15

and how to compensate for it. This results in that the correct counter actions were carried out to maintain stability. However the driver tried not to use any steering until it was necessary.

6.1.2 Test Results

The test results is divided based on the initial velocity, also a summary of all test is presented. The results can be seen in Tab. 6.1-6.4.

6.1.3 Kinematic Detector

The results of the μ-split detector can be seen in Tab. 6.1-6.4. The fastest detection is 0.08 s while the slowest is 0.22 s, with an average of 0.14 s. While the kinematic detector shows great results in detection of μ-split situations the robustness is poor, with a high risk of false detection during non μ-split situations. This is the reason that an additional logic was implemented as mentioned in Sec. 3.2.1. With the additional logic the detector becomes more robust with only one false detection as can be seen in Tab. 6.3. As seen in Fig. 6.1, even though this is not a μ-split situation it shows some clear signs of μ-split behavior at the end of the braking, which is the reason for the false detection. The increased robustness will however give a slower detection time when the additional logic is activated. This

Table 6.3: *Test results from low-μ robustness braking. A number indicates the time for false detection and a dash indicates no detection.*

Detector	Initial Velocity 30 km/h	50 km/h	70 km/h
Kinematic	0.64	1.30	-
	0.60	2.30	-
	-	1.61	-
Kinematic With Additional Logic	-	-	7.61
	-	-	
	-	-	-
Dynamic	-	-	-
	-	-	-
	-	-	

Table 6.4: *Summary of all test.*

	Unit	Kinematic	Kinematic with Additional Logic	Dynamic
Mean Detection Time	[s]	0.14	0.14	0.25
Best Detection Time	[s]	0.08	0.08	0.18
Worst Detection Time	[s]	0.22	0.22	0.41
Missed Detection	[%]	0	0	11
False Detection	[%]	56	11	0

can be seen in Tab. 6.2 where the additional logic has been tested separately on the μ-split data.

Dynamic Detector

In Tab. 6.4 it can be seen that the dynamic detector can detect a μ-split braking situation after 0.25 s on average. However the detection time can be significantly slower but not significantly faster with the slowest time at 0.41 s and the fastest at 0.18 s. The detector shows high robustness with a low chance of false detection.

In Tab. 6.4 it can be seen that there is a probability of missed detection. By looking at Tab. 6.1 the results show that the detector missed one detection with an initial velocity of 30 km/h. This can be explained by looking at Fig. 6.2 where T_{pos} from (3.3) are shown for different tests. By looking at this signal it can clearly be seen from the Fig. 6.2a and 6.2b that it is harder to distinguish a μ-split braking from a normal braking situation at lower velocities. While Fig. 6.2c-6.2f shows that there will be a significant difference in the reactions for higher velocities.

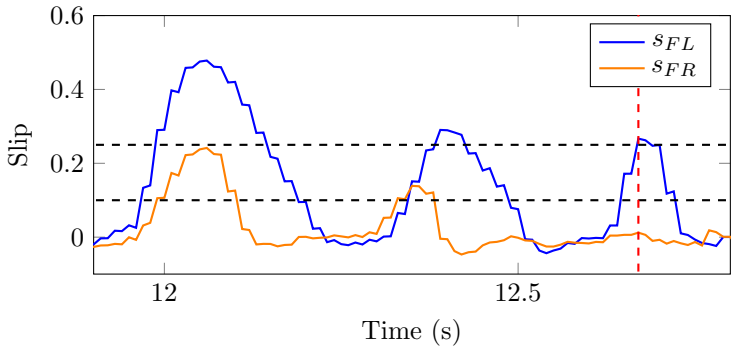

Figure 6.1: *The figure shows a low-μ braking from 70 km/h where the kinematic detector gives a false detection. The detection is made at the red dotted line.*

6.2 Controller Results

The controllers were tested on several μ-split braking situations in the simulation environment. The longitudinal force used as input to the simulation is based on real test measurements from μ-split braking taken at a test track. The tests were performed with different initial velocities and with the same vehicle setup as in Sec. 6.1.1. The measured longitudinal acceleration was used in (4.3) to compute the input force. The friction coefficients used as input to the simulation are $\mu_{left} = 0.8$ and $\mu_{right} = 0.2$, these are the assumed values of the friction at the test track. All test cases are validated as done in Sec. 4.2 and they are labeled 1-8. The reason that there are several test at each initial velocity is to ensure that the data is consistent. Since the inputs to the simulation are based on measured signals the results from the simulation environment will have small variations for the same initial velocity. The reason for this is that there will be variations in the measured longitudinal acceleration between different test cases with the same initial velocity.

For the tests of the AYC, it is not activated until the μ-split situation is detected, until the detection is done the PF is active. The detection time is based on the mean value in detection time of the dynamic detector that can be found in Tab. 6.4. The reason that the dynamic detector is used is that it has the slowest detection time, which gives a worse scenario compared to a faster detector.

6.2.1 Test Results

The maximum, average and standard deviation of the absolute values of the path errors are computed for each test. These values are presented for each controller and test and can be seen in Tab. 6.5-6.7. In addition to this a summary can be found in Tab. 6.8. In Fig. 6.3 the error signals from test number 1 can be seen together with the yaw rate and steering angle. In Fig. 6.4 test number 3 is shown since it gave the worst results for every controller.

Path Follower Normal Tuning

In Tab. 6.5 it can be seen that the maximum and average lateral deviation is in similar size for the corresponding initial velocity. The average and maximum heading error increases for smaller initial velocities compared to higher initial velocities. By looking at Fig. 6.3 and 6.4 it can be seen that the behavior of the controller is similar for both tests. Initial there is a peak in the yaw rate leading to an heading error which results in an lateral error. In Fig. 6.3 the controller manages to decrease the heading error which leads to a smaller error in lateral deviation. In Fig. 6.4 the controller does not manage to decrease the heading error resulting in a larger lateral error.

Path Follower μ-split Tuning

As seen in Tab. 6.6, Fig. 6.3 and 6.4. the heading error follows the same pattern as for the PF while the lateral deviation is smaller. The overall behavior is much like the one of the PF, with a slightly more aggressive steering. Resulting in a smaller lateral deviation and a more variations in heading error.

Path Follower with Active Yaw Control

In Tab. 6.7 it can be seen that both the lateral deviation and the heading error follows almost the exact behavior of the PF. Which one would expect since the AYC based on the PF. The difference can be seen in Fig. 6.3 and 6.4. The initial behavior is similar to the PF, but after the initial compensation the steering is smoother. This leads to a smoother behavior in the heading error and the yaw rate. The lateral deviation is about the same as for the PF in the 70 km/h test, while the lateral deviation is lower in the 50 km/h test.

Table 6.5: *The table shows the results from using the PF on different μ-split braking tests.*

		Lateral Deviation			Heading Error		
Test	Init. Vel. [km/h]	Max [m]	Avg. [m]	Std. [m]	Max [deg]	Avg. [deg]	Std. [deg]
1	70	0.040	0.025	0.013	0.79	0.42	0.19
2	70	0.042	0.026	0.013	0.77	0.43	0.20
3	50	0.048	0.030	0.017	1.43	0.88	0.30
4	50	0.051	0.032	0.018	1.03	0.83	0.22
5	50	0.048	0.030	0.017	1.17	0.82	0.23
6	30	0.021	0.010	0.0062	1.39	0.93	0.37
7	30	0.021	0.010	0.0065	1.29	0.92	0.35
8	30	0.016	0.0087	0.0053	1.31	0.86	0.36
Avg.	-	0.036	0.021	0.012	1.15	0.76	0.28

Table 6.6: *The table shows the results from using the PFX on different μ-split braking tests.*

		Lateral Deviation			Heading Error		
Test	Init. Vel. [km/h]	Max [m]	Avg. [m]	Std. [m]	Max [deg]	Avg. [deg]	Std. [deg]
1	70	0.020	0.012	0.0056	0.80	0.42	0.18
2	70	0.020	0.013	0.0054	0.78	0.42	0.19
3	50	0.024	0.016	0.0068	1.40	0.87	0.30
4	50	0.025	0.018	0.0075	1.00	0.80	0.21
5	50	0.024	0.016	0.0071	1.14	0.79	0.22
6	30	0.015	0.0083	0.0043	1.34	0.91	0.36
7	30	0.015	0.0086	0.0047	1.25	0.90	0.34
8	30	0.012	0.0073	0.0039	1.27	0.84	0.34
Avg.	-	0.019	0.012	0.0057	1.12	0.74	0.27

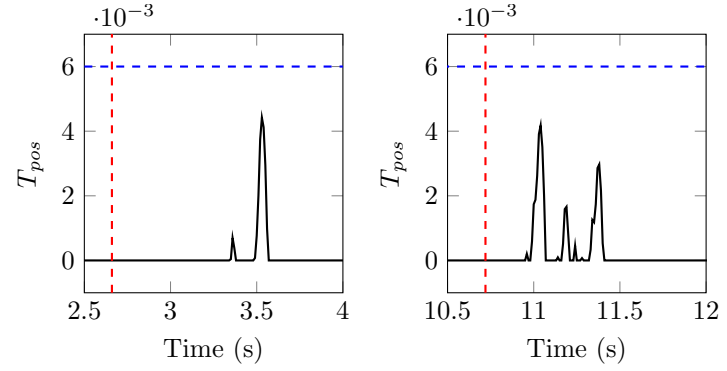

(a) *Low-μ braking at 30 km/h.* **(b)** *μ-split braking at 30 km/h.*

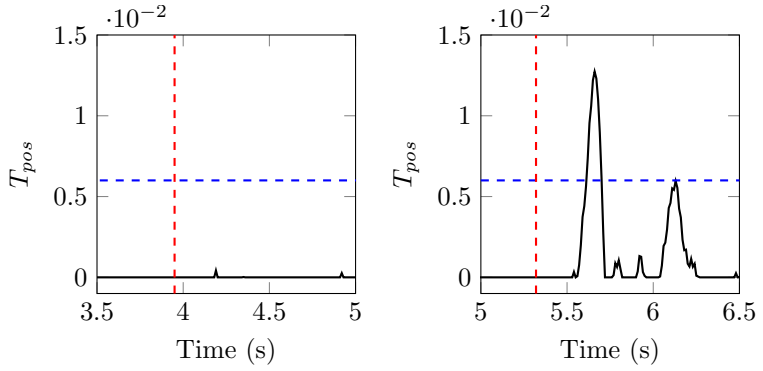

(c) *Low-μ braking at 50 km/h.* **(d)** *μ-split braking at 50 km/h.*

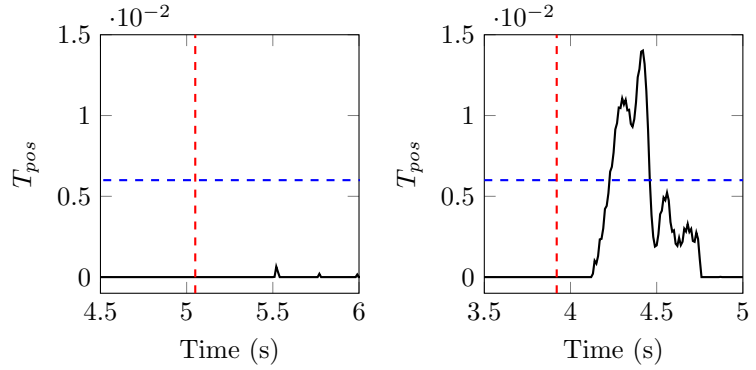

(e) *Low-μ braking at 70 km/h.* **(f)** *μ-split braking at 70 km/h.*

Figure 6.2: *The figure shows the test signal T_{pos} for several different cases. The red line shows the start of braking and the blue line shows the fixed limit in the CUSUM algorithm.*

Table 6.7: *The table shows the results from using the PF with the AYC on different μ-split braking tests.*

		Lateral Deviation			Heading Error		
Test	Init. Vel. [km/h]	Max [m]	Avg. [m]	Std. [m]	Max [deg]	Avg. [deg]	Std. [deg]
1	70	0.041	0.026	0.013	0.77	0.42	0.19
2	70	0.042	0.027	0.013	0.75	0.43	0.20
3	50	0.044	0.026	0.014	1.33	0.87	0.28
4	50	0.047	0.029	0.017	1.00	0.82	0.22
5	50	0.045	0.027	0.016	1.09	0.81	0.22
6	30	0.011	0.0063	0.0029	1.31	0.89	0.36
7	30	0.012	0.0067	0.0034	1.24	0.89	0.35
8	30	0.012	0.0054	0.0035	1.24	0.83	0.35
Avg.	-	0.032	0.019	0.010	1.09	0.75	0.27

Table 6.8: *The table shows a summary of the average values for each controller from the simulations.*

	Lateral Deviation			Heading Error		
	Max [m]	Avg. [m]	Std. [m]	Max [deg]	Avg. [deg]	Std. [deg]
PF	0.036	0.021	0.012	1.15	0.76	0.28
PFX	0.019	0.012	0.0057	1.12	0.74	0.27
AYC	0.032	0.019	0.010	1.09	0.75	0.27

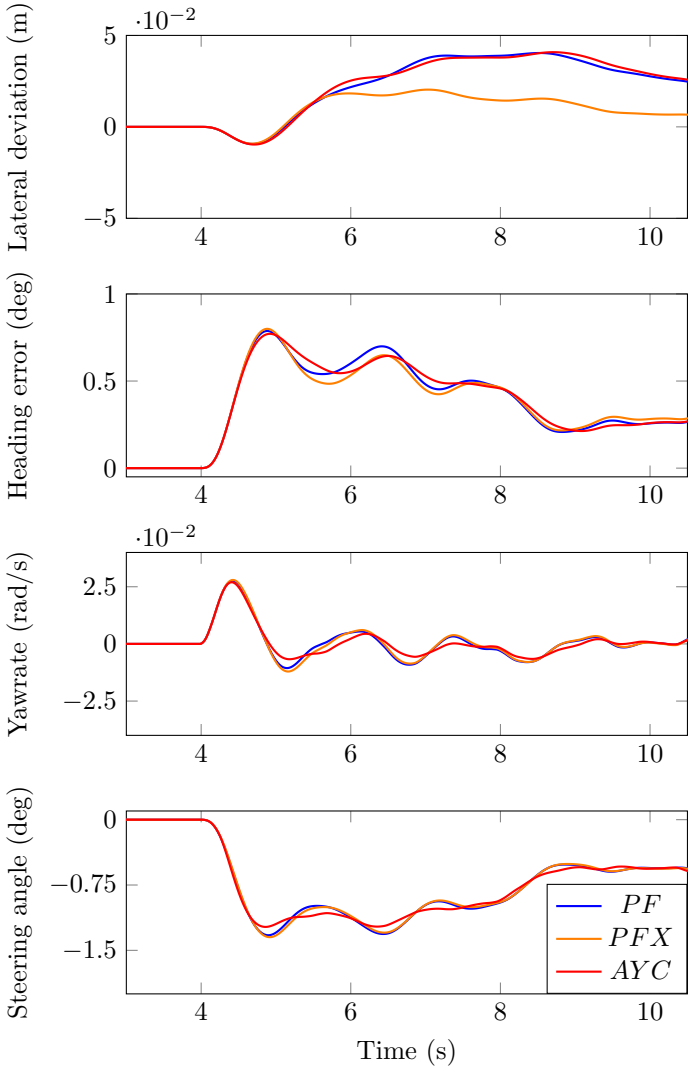

Figure 6.3: *The figure shows the path errors, the yaw rate and the steering angle for each controller during a μ-split braking with a initial velocity of 70 km/h.*

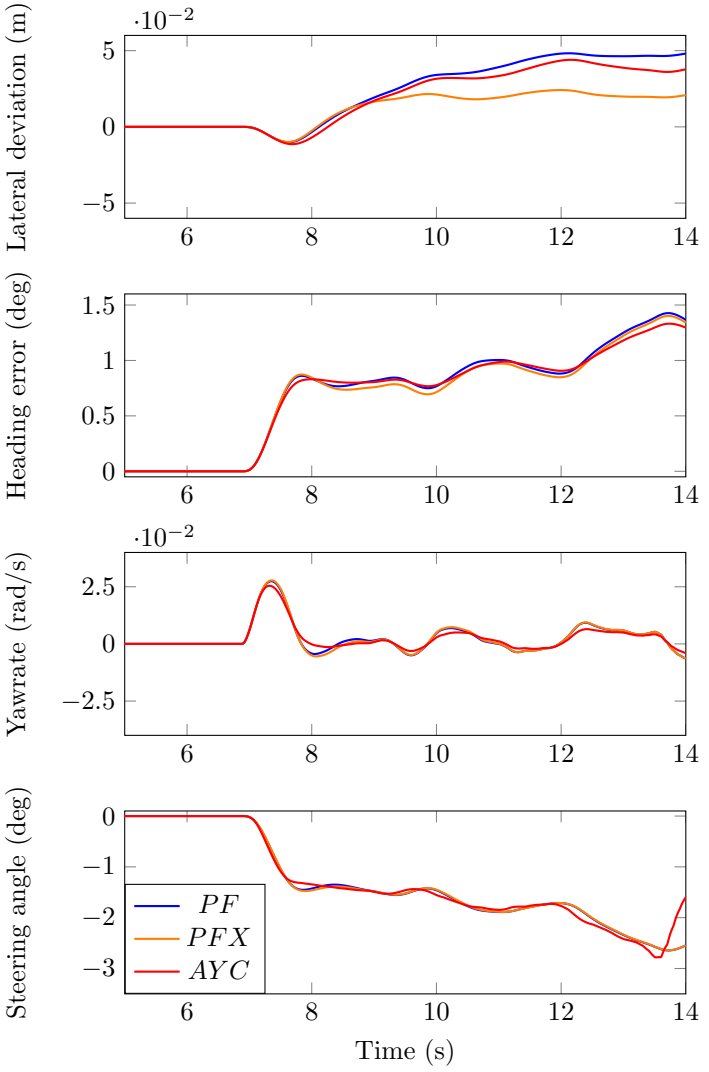

Figure 6.4: *The figure shows the path errors, the yaw rate and the steering angle for each controller during a μ-split braking with a initial velocity of 50 km/h.*

7

Discussion and Conclusions

In this chapter the results from the μ-split detectors and control strategies are analyzed. Conclusions and suggestions for future work are presented based on the results.

7.1 Detection of μ-Split Situations

When comparing the kinematic detector to the dynamic detector the results show that the kinematic detector is faster but the dynamic detector is more robust. In terms of complexity the kinematic detector is less complex with less parameters to tune, while the dynamic detector has more parameters to tune.

7.1.1 Detection time

By looking at Tab. 6.4 it can be seen that the kinematic detector is on average almost twice as fast as the dynamic detector. When comparing the best and worst detection time the kinematic detector is even faster compared to the dynamic detector. This can be explained by the fact that the kinematic detector uses sensor data from the wheels, where a μ-split situation is expected to be seen in the first ABS control cycle. The dynamic detector uses data from the yaw rate sensor to detect a μ-split situation. The unexpected yaw torque is a consequence from the ABS system and the forces acting on the wheels and that is the main reason why it is slower compared to the kinematic detector. Also, the dynamic detector uses filtering, SMO and CUSUM algorithm, which will give a time delay compared to the kinematic detector which does not use any filtering.

7.1.2 Robustness

By looking in Tab. 6.4 it can be seen that the dynamic detector has high robustness compared to the kinematic detector. Since the kinematic detector only uses raw sensor data from the wheels, sudden changes in the data will lead to large variations in the slip values which can lead to false detections. The reason that the dynamic detector shows greater robustness is, as mentioned before, that the yaw rate is a consequence of the forces acting on the wheels. Due to the inertia of the vehicle these sudden changes will only give small variations in the yaw rate leading to the high robustness of the dynamic detector. The robustness is further improved by the filtering from the SMO and the CUSUM algorithm in the detector.

When the additional logic was added to the kinematic detector its robustness increased, as seen in Tab. 6.4. With the additional logic the detector only has one false detection compared to earlier with five false detections. With the additional logic the problems discussed in Sec. 3.2.1 are solved. But there are still cases when the raw data show a μ-split like behavior, as seen in Fig. 6.1, which will lead to false detection.

7.1.3 Complexity

The kinematic detector has a simple algorithm where sensor data is used. This algorithm can be implemented and used with minimal tuning. When adding the additional logic the algorithm remains simple, however additional tuning has to be done. The dynamic detector is more complex and has several parameters that has to be tuned. As can be seen in Fig. 6.2 the tuning of the CUSUM algorithm at low velocities is hard since the reactions from a μ-split braking is similar to a low-μ braking. The SMO uses a singe-track model, which has several parameters. Many of them such as lengths and weight are easy to determine while parameters such as the cornering stiffness is not easy to estimate and contains uncertainties.

7.2 Steering Control During µ-split Braking

As discussed in Sec. 5.1 the steering behavior during μ-split braking is contradictory. This contradiction is an issue concerning path following. The reason that this is a problem is that the steady state behavior introduces a fairly large body slip on the vehicle, while it is only possible to get zero heading error and zero lateral deviation at the same time under the assumption that the body slip is zero as described in Sec. 2.1.1. As described in Sec. 5.1 this was a problem for the driver since it is not intuitive to drive with a constant body slip, but it is also not intuitive to have a yawing motion on the vehicle during straight line braking. The problem of keeping the lateral error and heading error equal to zero also occurred during simulations. As seen in Fig. 6.3 and 6.4 none of the controllers managed to reduce the errors to zero due to this contradiction.

7.2.1 Controller Performance

As seen in Fig. 6.3 and Fig. 6.4 the controller manages to find a fairly steady state behavior. The steady state behavior does not mean that the lateral deviation and heading error are equal to zero. This behavior is similar to the behavior explained in Sec. 5.1.1, where the desired behavior during a μ-split situation is to have a non zero body slip angle and steering angle. The behavior of the PF can be compared to a drivers behavior. The driver over compensates the steering angle when trying to keep the heading error to zero and maintain lateral stability at the same time, this leads to the nervous behavior seen in Fig. 5.1. The driver can not do both due to the contradiction in Sec. 5.1. The PF manages to keep the vehicle at a more steady behavior with a body slip angle, however it does not keep the path errors to zero. The conclusion is that the PF has the desired behavior described in Sec. 5.1.1 but the downside is that the path errors do not converge to zero due to the reason mentioned in Sec. 2.1.1.

The desired behavior can be improved further by changing the weighting factors of the controller which has been done for the PFX. By increasing the weighting factor for the lateral error and decreasing the weighting factor for the heading error, the controller allows more deviation in heading error to keep the lateral deviation small. This reduces the effects the body slip has on the lateral deviation as described in Sec. 2.1.1. The improvements can be seen in Fig. 6.3 and 6.4 where the lateral deviation is clearly reduced while the heading error remains at the same level.

The behavior can also be improved by the addition of two other control parameters: yaw rate and body slip. This is used in the AYC, the result is similar to the PF which it is based on. By also minimizing the yaw rate a smoother steering angle is generated leading to a calmer behavior during the μ-split braking as seen in Fig. 6.3 and 6.4. In the figures it can also be seen that the yaw rate is less oscillatory, indicating a calmer motion. Similar results would be achieved if the AYC was based on the PFX.

7.3 Combination of Detector and Controller

During a μ-split braking one method to get a better behavior could be to change the control strategy after a detection. As shown in the simulations a AYC or the PFX had better performance compared to the PF. By introducing a change in the control strategy after a detection the effects of a missed detection or a false detection has to be analyzed.

7.3.1 Consequences of Missed Detection

The consequences of a missed detection depends on how good the normal PF handles a μ-split situation. If the controller can not handle the situation a missed detection can lead to an accident. If the PF can handle the situation the consequence could be a loss in performance but it would not lead to an accident. The

conclusion of the consequences of a missed detection comes down to a discussion of the performance of the normal PF. Based on the test result of the PF the consequence would be worse performance compared to the PFX and the AYC. These results can not be used to ensure stability in real life.

7.3.2 Consequences of False Detection

A false detection could result in a situation where a normal safe braking becomes unstable leading to an accident. This depends on how well the alternative control strategy handles a normal braking. The steady state behavior during a normal braking with the same friction on the left and right side of the vehicle can be analyzed the same way as done in Sec. 5.1.1. The difference between a normal braking and a μ-split braking is that there will be no unexpected torque, M_{un}. By looking at (5.5) and (5.6) it can be seen that the steady state will have $\delta_{ss} = 0$ and $\beta_{ss} = 0$ and there will be no contradiction in steering behavior. If the AYC is used it will try to control the body slip to zero which is the desired steady state. If M_{un} is zero the error between wanted yaw rate from the PF and the measured yaw rate should be small and converge to zero as heading error converges to zero. When it comes to switching to an alternative controller tuning, in this case PFX the consequences depends on how the controller is tuned, as long as the tuning is validated on normal braking this should not be a problem.

7.4 Conclusions

The PF performs well in the simulation environment but since the simulation environment can not describe a μ-split situation perfect, as discussed in Sec. 4.2.3, conclusions about the stability in real life can not be made. The controller shows a behavior that has potential to handle a μ-split braking in real life. By introducing a different control strategy during a μ-split situations the performance and stability of the vehicle can be further improved according to the results from the simulation. The most important conclusion is that a controller that can handle a non zero body slip seems to handle the situation better.

The simulation results of the controller show that a controller can handle the situation without a detector. This means that there is no need for the detector to be sufficiently fast. However a detector could be used to improve the handling during a μ-split braking by changing the control strategy. A fast detection allows for a faster change in control strategy which gives a better result during the μ-split braking. As discussed in Sec. 7.3.2 there seems to be no dangerous consequences of a false detection and therefore the speed of the detector is more important than the robustness resulting in that the kinematic is more suitable.

7.5 Future Work

Since the thesis concludes that the steering behavior of a PF is reasonable during μ-split braking and that the simulations shows a stable behavior. To draw further conclusions about the ability of a PF to handle μ-split braking the next step would be real life tests. The results could also be used to further validate the simulation model.

The problem that the body slip affects the path following problem should be further investigated. A reasonable approach could be to use the μ-split detector to include the body slip in the path errors. This could result in a lower lateral deviation and a smoother steering behavior.

As shown in Sec.5.1.1 the size of the unwanted torque, M_{un}, is an important factor in the vehicle behavior. An estimate of M_{un} could be used to detect a μ-split situation. It could also be used in a AYC to computed a non zero body slip reference by using (5.5) and (5.6).

This thesis only considers a tractor during straight line braking with homogeneous μ-split and without a trailer. A further investigation should be done without these limitations. In real life the surface often varies with time and braking occurs in corners, this effects both the detector and the controller and should be investigated. When a trailer is attached to the tractor the stability of the vehicle also includes the stability of the trailer. This has to be considered when steering and should be further investigated.

Investigate if a better overall performance could be achieved by combining the lateral and longitudinal control of the vehicle. The objective for this controller would be to minimize the braking distance and the lateral deviation. The main advantage with this method is that by coordinating the braking and the steering a better overall performance during μ-split braking could be achieved.

Appendix

A

Appendix

A.1 Sliding Mode Observer Model

Equation (2.2) is used with the addition of an unexpected force, F_{un}, and unexpected torque, M_{un}. Leading to

$$\begin{aligned} m(\dot{v}_y + v_x\Omega) &= 2C_{\alpha r}\alpha_r + 2C_{\alpha f}\alpha_f \cos(\delta) + F_{xf}\sin(\delta) + F_{un} \\ I_z\dot{\Omega} &= l_f(2C_{\alpha f}\alpha_f \cos(\delta) + F_{xf}\sin(\delta)) - l_r 2C_{\alpha r}\alpha_r + M_{un} \end{aligned} \tag{A.1}$$

Equation (2.3) is used to replace the slip angles and with the assumption of small angles the following equations are derived

$$\begin{aligned} \dot{v}_y &= \overbrace{-\frac{2C_{\alpha f} + 2C_{\alpha r}}{mv_x}}^{a_1} v_y \overbrace{-\left(v_x + \frac{2l_f C_{\alpha f} - 2l_r C_{\alpha r}}{mv_x}\right)}^{a_2}\Omega + \overbrace{\frac{2C_{\alpha f}}{m}}^{b_1}\delta \; \overbrace{-\frac{1}{m}}^{e_1} F_{un} \\ \dot{\Omega} &= \underbrace{-\frac{2l_f C_{\alpha f} - 2l_r C_{\alpha r}}{I_z v_x}}_{a_3} v_y \underbrace{-\frac{2l_f^2 C_{\alpha f} + 2l_r^2 C_{\alpha r}}{I_z v_x}}_{a_4}\Omega + \underbrace{\frac{2l_f C_{\alpha f}}{I_z}}_{b_2}\delta \; \underbrace{-\frac{1}{I_z}}_{e_2} M_{un} \end{aligned} \tag{A.2}$$

By solving the first equation for v_y and replacing v_y in the second equation and then differentiate the first equation with the assumption of constant longitudinal

velocity the follow equations are obtained

$$\begin{aligned}\ddot{v}_y &= a_1\dot{v}_y + a_2\dot{\Omega} + b_1\dot{\delta} + e_1\dot{F}_{un}\\ \dot{\Omega} &= \frac{a_3}{a_1}\dot{v}_y + \left(a_4 - \frac{a_2a_3}{a_1}\right)\Omega + \left(b_2 - \frac{a_3b_1}{a_1}\right)\delta + e_2M_{un} - \frac{a_3e_1}{a_1}F_{un}\end{aligned} \tag{A.3}$$

Finally Ω in the first equation are substituted by the second equation resulting in

$$\begin{aligned}\ddot{v}_y &= \left(a_1 + \frac{a_2a_3}{a_1}\right)\dot{v}_y + \left(a_2a_4 - \frac{a_2^2a_3}{a_1}\right)\Omega + \left(a_2b_2 - \frac{a_2a_3b_1}{a_1}\right)\delta + b_1\dot{\delta} - \frac{a_2a_3e_1}{a_1}F_{un}\\ &\quad + e_1\dot{F}_{un} + a_2e_eM_{un}\\ \dot{\Omega} &= \frac{a_3}{a_1}\dot{v}_y + \left(a_4 - \frac{a_2a_3}{a_1}\right)\Omega + \left(b_2 - \frac{a_3b_1}{a_1}\right)\delta + e_2M_{un} - \frac{a_3e_1}{a_1}F_{un}\end{aligned} \tag{A.4}$$

In matrix form

$$\begin{aligned}\underbrace{\begin{bmatrix}\ddot{v}_y\\ \dot{\Omega}\end{bmatrix}}_{\dot{x}} &= \underbrace{\begin{bmatrix}\left(a_1 + \frac{a_2a_3}{a_1}\right) & \left(a_2a_4 - \frac{a_2^2a_3}{a_1}\right)\\ \frac{a_3}{a_1} & \left(a_4 - \frac{a_2a_3}{a_1}\right)\end{bmatrix}}_{A}\underbrace{\begin{bmatrix}\dot{v}_y\\ \Omega\end{bmatrix}}_{x} + \underbrace{\begin{bmatrix}\left(a_2b_2 - \frac{a_2a_3b_1}{a_1}\right) & b_1\\ \left(b_2 - \frac{a_3b_1}{a_1}\right) & 0\end{bmatrix}}_{B}\underbrace{\begin{bmatrix}\delta\\ \dot{\delta}\end{bmatrix}}_{u}\\ &\quad + \underbrace{\begin{bmatrix}-\frac{a_2a_3e_1}{a_1} & e_1 & a_2e_e\\ -\frac{a_3e_1}{a_1} & 0 & e_2\end{bmatrix}}_{F}\begin{bmatrix}F_{un}\\ \dot{F}_{un}\\ M_{un}\end{bmatrix}\end{aligned} \tag{A.5}$$

Bibliography

[1] J. Ackermann and T. Bünte. Yaw disturbance attenuation by robust decoupling of car steering. *Control Engineering Practice*, 5:1131–1136, 10 1999. doi: 10.1016/S0967-0661(97)00106-8.

[2] C. Ahn, B. Kim, and M. Lee. Modeling and control of an anti-lock brake and steering system for cooperative control on split-mu surfaces. *International Journal of Automotive Technology*, 13, 06 2012. doi: 10.1007/s12239-012-0055-y.

[3] Michèle Basseville, Igor V Nikiforov, et al. *Detection of abrupt changes: theory and application*, volume 104. prentice Hall Englewood Cliffs, 1993.

[4] S. Drakunov and V. Utkin. Sliding mode observers. tutorial. In *Proceedings of 1995 34th IEEE Conference on Decision and Control*, volume 4, pages 3376–3378 vol.4, Dec 1995. doi: 10.1109/CDC.1995.479009.

[5] C. Edwards, Roderick Hebden, and S.K. Spurgeon. Sliding mode observers for vehicle mode detection. *Vehicle System Dynamics*, 43:823–843, 11 2005. doi: 10.1080/00423110500225855.

[6] Torkel Glad and Lennart Ljung. *Reglerteori : flervariabla och olinjära metoder*. Studentlitteratur, Lund, 2. uppl. edition, 2003. ISBN 9144030037.

[7] Fredrik Gustafsson. Slip-Based Estimation of Tire-Road Friction. *Automatica*, 33(6):1087–1099, 1997.

[8] Xiangkun He, Kaiming Yang, Liu Yulong, and Xuewu Ji. A novel direct yaw moment control system for autonomous vehicle. 08 2018. doi: 10.4271/2018-01-1594.

[9] C. Hu, R. Wang, F. Yan, and N. Chen. Should the desired heading in path following of autonomous vehicles be the tangent direction of the desired path? *IEEE Transactions on Intelligent Transportation Systems*, 16(6):3084–3094, 2015.

[10] Chuan Hu, Rongrong Wang, Fengjun Yan, and M. Chadli. Composite nonlinear feedback control for path following of four-wheel independently actu-

ated autonomous ground vehicles. volume 17, 12 2015. doi: 10.1109/TITS.2015.2498172.

[11] M. Keshavarz Bahaghighat, S. Kharrazi, M. Lidberg, P. Falcone, and B. Schofield. Predictive yaw and lateral control in long heavy vehicles combinations. In *49th IEEE Conference on Decision and Control (CDC)*, pages 6403–6408, Dec 2010. doi: 10.1109/CDC.2010.5717377.

[12] Paul Lin, Maosheng Ye, and Kuo-Ming Lee. Intelligent observer-based road surface condition detection and identification. pages 2465–2470, 10 2008. doi: 10.1109/ICSMC.2008.4811665.

[13] Jadranko Matuško, Ivan Petrovic, and Nedjeljko Peric. Neural network based tire/road friction force estimation. *Engineering Applications of Artificial Intelligence*, 21:442–456, 04 2008. doi: 10.1016/j.engappai.2007.05.001.

[14] M. Meywerk. *Vehicle Dynamics*. Automotive Series. Wiley, 2015. ISBN 9781118971352.

[15] Mattias Nyberg and Erik Frisk. Model based diagnosis of technical processes. Course Compendium in TSFS06 at Linköping university.

[16] B. Paden, M. Čáp, S. Z. Yong, D. Yershov, and E. Frazzoli. A survey of motion planning and control techniques for self-driving urban vehicles. *IEEE Transactions on Intelligent Vehicles*, 1(1):33–55, March 2016. ISSN 2379-8858. doi: 10.1109/TIV.2016.2578706.

[17] Joop P. Pauwelussen. Chapter five - vehicle handling performance. In Joop P. Pauwelussen, editor, *Essentials of Vehicle Dynamics*, pages 123 – 194. Butterworth-Heinemann, Oxford, 2015. ISBN 978-0-08-100036-6. doi: https://doi.org/10.1016/B978-0-08-100036-6.00005-4. URL `http://www.sciencedirect.com/science/article/pii/B9780081000366000054`.

[18] Hebden R.G, C. Edwards, and S.K. Spurgeon. Automotive steering control in a split- manoeuvre using an observer-based sliding mode controller. *Vehicle System Dynamics*, 41:181–202, 01 2004. doi: 10.1076/vesd.41.3.181.26511.

[19] Bruno Siciliano and Oussama Khatib. *Springer Handbook of Robotics*. Springer-Verlag, Berlin, Heidelberg, 2007. ISBN 354023957X.

[20] Zhu Tianjun and Zong Changfu. Modelling and active safe control of heavy tractor semi-trailer. volume 2, pages 112 – 115, 11 2009. doi: 10.1109/ICICTA.2009.264.

[21] J.Y. Wong. *Theory of Ground Vehicles*. Wiley, 4 edition, 2008. ISBN 9780470170380.

[22] Shu Zhou, Si Zhang, and Guang Zhao. Stability control on tractor semi-trailer during split-mu braking. *Advanced Materials Research*, 230-232: 549–553, 05 2011. doi: 10.4028/www.scientific.net/AMR.230-232.549.